Molecular Therapy
Original Article

AAT-MSC-EVs: Novel implications for suppressing ferroptosis, fibrosis and pain associated with chronic pancreatitis

Sara Shoeibi,[1] Wenyu Gou,[1] Tiffany Yeung,[1] Kristi Helke,[2] Erica Green,[1] Charlie Strange,[3,4] and Hongjun Wang[1,4]

[1]Department of Surgery, Medical University of South Carolina, Charleston, SC 29425, USA; [2]Department of Comparative Medicine, Medical University of South Carolina, Charleston, SC 29425, USA; [3]Department of Medicine, Medical University of South Carolina, Charleston, SC 29425, USA

Chronic pancreatitis (CP) is characterized by inflammation, acinar cell death, fibrosis, and persistent pain. We investigated mesenchymal stem/stromal cell (MSC)-derived extracellular vesicles (EVs) for CP treatment. CP was modeled in male mice using bile duct TNBS infusion, and pancreatic tissues from CP patients were also analyzed. EVs from immortalized human MSCs overexpressing alpha-1 antitrypsin (iAAT-MSCs) were tested for their effects on ferroptosis, fibrosis, and pain. CP tissues showed reduced glutathione peroxidase 4 (GPx4) activity ($p < 0.05$) and iron accumulation, indicating ferroptosis. iMSC and iAAT-MSC-EVs alleviated CP symptoms by suppressing ferroptosis, restoring GPx4 activity, reducing MDA levels, and mitigating fibrosis markers (α-smooth muscle actin, transforming growth factor-β1, matrix metalloproteinase 2). EV treatment also alleviated pain by decreasing macrophage and mast cell infiltration into the pancreas and dorsal root ganglia while reducing pain-related gene expression (TRVP1, TacR1, Necab3). Additionally, iAAT-MSC-EVs were distinct in cytokine signaling, PI3K-Akt pathway activation, and upregulation of miRNAs like miR-9, miR-10a-5p, miR-92a, miR-200, miR-370, and miR-146a. These results suggest ferroptosis as a key mechanism in CP and highlight the therapeutic potential of iAAT-MSC-EVs in addressing ferroptosis, fibrosis, and pain, presenting a promising, cell-free therapeutic strategy for CP.

INTRODUCTION

Chronic pancreatitis (CP) is a progressive inflammatory condition characterized by prolonged pancreatic inflammation.[1,2] Persistent inflammation is associated with the destruction of pancreatic tissue, pancreatic fibrosis, and atrophy.[3] The loss of organ function likely involves complex mechanisms that ultimately result in chronic pain.[1,4] However, the poorly understood pathophysiology of CP makes it challenging to identify the means to treat the underlying cellular disorder.

Ferroptosis is a newly recognized pathway of regulated cell death resulting from iron accumulation and lipid peroxidation. An imbalance in oxidant stress and antioxidant protection with enzymes such as glutathione peroxidase 4 (GPx4) and superoxide dismutase type 1 (SOD1) eventually leads to cell death.[5] During chronic inflammation, the pancreas experiences oxidative stress, causing an overload of intracellular iron and initiating the Fenton reaction, ultimately leading to lipid peroxidation and the generation of reactive oxygen species (ROS).[6–8] These processes likely contribute to the destruction of pancreatic tissue and exacerbate the inflammatory response, further perpetuating the condition. Experimental studies have demonstrated that targeting ferroptosis can alleviate pancreatic injury and inflammation severity in animal models of acute pancreatitis.[9–11] However, it is largely unknown whether ferroptosis contributes to acinar cell death in CP patients and TNBS-induced CP mice.

Pancreatic fibrosis, like fibrosis in other body organs, is characterized by the excessive deposition of extracellular matrix components that is likely facilitated by the activation and recruitment of inflammatory blood cells.[12,13] In addition, pancreatic stellate cells (PSCs) and pancreatic acinar cells may contribute to fibrotic pathways, although their contribution is not fully explored. The extent to which inflammation and fibrosis are pathogenetically linked to neuronal sensitization and damage responsible for chronic pain, another key feature of CP, is also unknown.[2,13–15] Gaining a comprehensive understanding of these intricate connections is essential for developing effective therapeutic strategies.

Mesenchymal stem/stromal cells (MSCs), both in culture and within the body, release small vesicles known as extracellular vesicles (EVs). These EVs contain a wide range of bioactive molecules, including proteins (such as enzymes, transcription factors, extracellular matrix proteins, and receptors), nucleic acids (including mtDNA, single-stranded DNA, double-stranded DNA, mRNA, and microRNA [miRNA]), and lipids. These components play a key role in the therapeutic efficacy of MSCs by mediating intercellular communication

Received 1 October 2024; accepted 18 March 2025;
https://doi.org/10.1016/j.ymthe.2025.03.028.

[4]Senior author

Correspondence: Hongjun Wang, Department of Surgery, Medical University of South Carolina, Charleston, SC 29425, USA.
E-mail: wangho@musc.edu

and influencing various biological processes. MSC-EVs exhibit therapeutic potential across various regenerative medicine and tissue engineering fields by regulating cellular processes and facilitating intercellular communication.[16,17] In numerous studies, EVs derived from MSCs have been investigated for their diagnostic and therapeutic capabilities in addressing the pathological processes associated with diabetes, respiratory diseases, and cardiovascular diseases.[18–20] The cargo of bioactive molecules within the MSC-EVs, notably growth factors and anti-inflammatory agents, plays a pivotal role in their therapeutic effects on damaged tissues.[21] Additionally, MSC-EVs possess anti-inflammatory properties, such as modulating immune response and diminishing tissue inflammation, that have notably been observed in pancreatic cancers.[22] In CP, the use of EVs derived from MSCs holds significant potential for diagnostic applications.[23] However, the question of whether EVs can be used for CP therapy and the mechanisms underlying their action remain largely unexplored.

Using MSC-EVs as a therapeutic alternative to cell therapies offers the advantage of a simplified manufacturing process for larger-scale interventions. While MSCs can be genetically modified, EVs from these cells can be assayed to ensure the appropriate expression of desired cellular products. In the current work context, MSCs have been engineered to overexpress human alpha-1 antitrypsin (AAT). This serine protease inhibitor is known to reduce inflammation and mitigate oxidative stress imbalance.[24,25] Additionally, the use of immortalized cell lines can result in infinitely reproducible clonal MSCs,[26] thereby enhancing the reliable and replicable production of therapeutic EVs.

This study characterized EVs derived from iAAT-MSCs by comparing them with EVs from normal immortalized MSCs (iMSCs) as controls. We analyzed the impact of these EVs on expression levels of miRNAs and mRNAs, predicted target genes, and potential biological functions. Additionally, the study explored differential expression markers between CP patients and normal individuals while exploring the therapeutic effects of iAAT-MSC-EVs in an *in vivo* TNBS-induced CP mouse model.

RESULTS

Characterization of iAAT-MSC-EVs

Human MSCs and AAT-MSCs were transduced with the SV40LT virus provided by the SV40 T Antigen Cell Immortalization kit (ALSTEM) to generate immortalized cells referred to as iMSCs and iAAT-MSCs. Both cells exhibited a similar fibroblast-like morphology under light microscopy. They showed expression of SV40 protein in immunofluorescent staining (Figure 1A). The size distribution of EVs derived from iMSCs and iAAT-MSCs ranged from 50 to 500 nm, with the majority having a diameter of approximately 150 nm (Figures 1B and 1C). Additionally, transmission electron microscopy (TEM) further confirmed the presence of EVs, showing their expected size and morphology (Figure 1D). Furthermore, EVs from both iMSCs and iAAT-MSCs expressed tetraspanin EV markers, including CD63, CD81, and CD9 (Figure 1E). Notably, the expression of human AAT protein was significantly increased in iAAT-MSC-derived EVs compared with iMSC-EVs (Figure 1E).

Treatment with iAAT-MSC-EVs reduces TNBS-induced pancreatic injuries

Previous studies have demonstrated that TNBS-treated rodent models manifest significant chronic inflammatory processes characterized by increased pancreas atrophy, collagen staining, fatty replacement, inflammation, and elevated histological pancreas damage scores.[27,28] To evaluate the therapeutic effects of EVs, male mice were randomly divided into four groups: the control group (sham operation with vehicle injection, control); TNBS, TNBS-induced CP mice receiving PBS injections; and iMSC-EV or iAAT-MSC-EV groups, CP mice treated with iMSC or iAAT-MSC-EVs. In the latter two groups, mice were injected with 200 μg of EVs via the tail vein at week 1, 2, and/or 3 weeks after TNBS treatment. Mice terminated at week 3 (group 1, two doses, short term) received 2 weekly doses of EVs, while those terminated at 6 weeks (group 2, three doses, long term) received three weekly doses of EVs (Figure 2A). There was a marked decrease in body weight after TNBS injection that lasted about 2 weeks. However, mice treated with iAAT-MSC-EVs showed a notably accelerated recovery in body weight compared with TNBS control or those treated with iMSC-EVs (Figure 2B).

The size of the pancreas in TNBS mice was significantly reduced compared with sham control mice at week 6 post TNBS infusions (Figure 2C). There were no significant differences in pancreas weight/body weight between the EV treatment groups vs. TNBS groups at 6 weeks post treatment (Figure 2D). The histological assessment of hematoxylin and eosin (H&E)-stained pancreas sections by a pathologist, who was blinded for group assignment, confirmed the presence of increased interlobular edema, inflammation, and necrosis in the pancreases of TNBS mice compared with the sham controls at three and six weeks after TNBS injection (Figures 2E–2I). TNBS mice receiving iAAT-MSC-EV showed significantly reduced interlobular edema, inflammation, and the most preserved area at 3 weeks compared with TNBS alone and iMSC-EV groups (Figures 2E–2G). Furthermore, mice receiving iMSC- or iAAT-MSC-EVs both demonstrated higher preservation of pancreatic tissue at week 6 compared with the TNBS group ($p < 0.05$) (Figure 2I). iAAT-MSC EV-treated mice also showed reduced interlobular edema and necrosis (Figures 2F, 2H and 2I), suggesting that treatment with iAAT-MSC-EVs reduces TNBS-induced pancreas injuries.

Evidence of iron deposition in CP patient pancreas and iAAT-MSC-EVs suppress iron accumulation in TNBS-treated mice

Ferroptosis, a form of regulated cell death characterized by iron-dependent lipid peroxidation, has been linked to various diseases, including acute pancreatitis and pancreatic cancer.[29,30] We hypothesize that ferroptosis could be an unrecognized mechanism of acinar cell death in CP (Figure 3A). To investigate this, we first

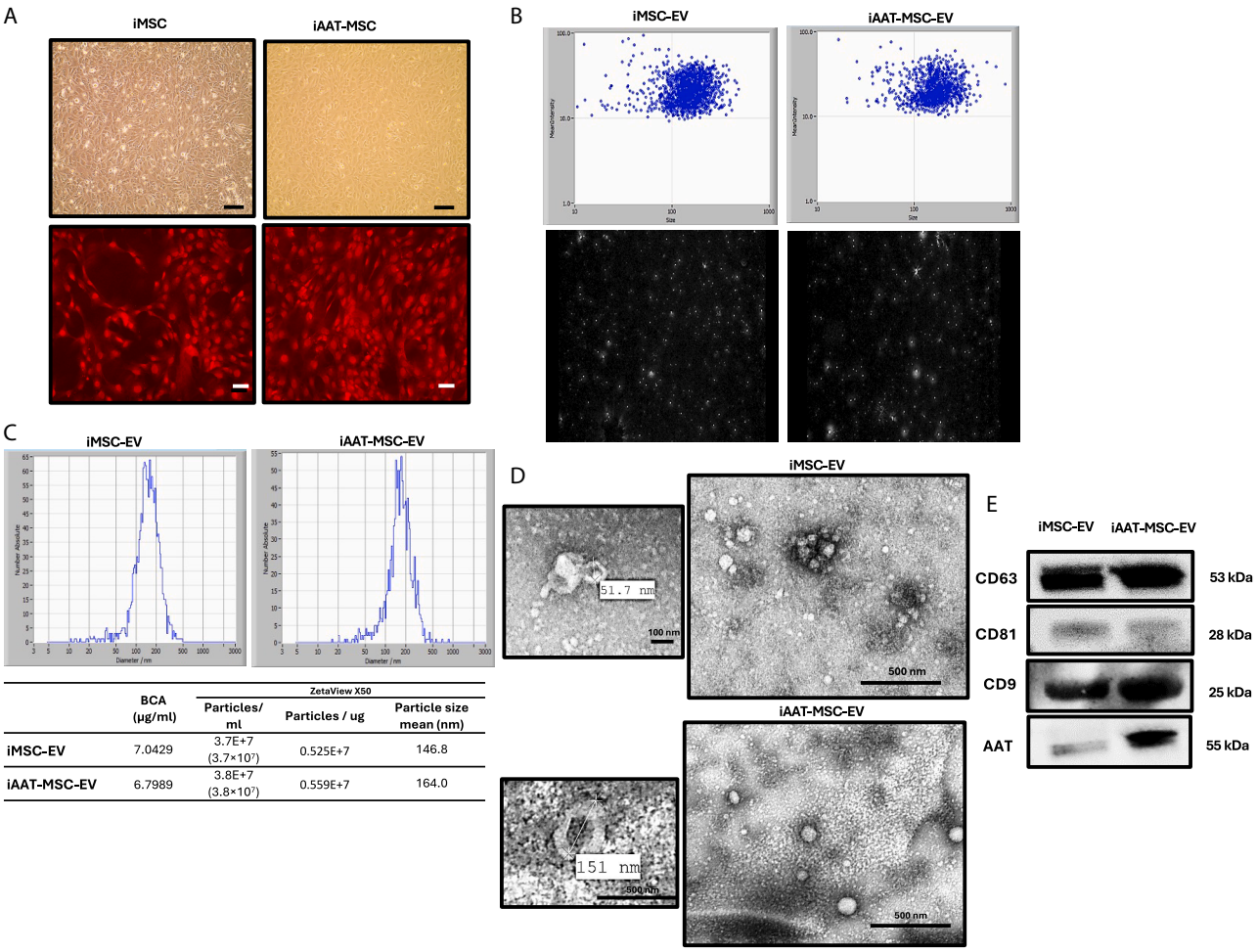

	BCA (μg/ml)	ZetaView X50 Particles/ml	ZetaView X50 Particles / ug	ZetaView X50 Particle size mean (nm)
iMSC-EV	7.0429	3.7E+7 (3.7×10⁷)	0.525E+7	146.8
iAAT-MSC-EV	6.7989	3.8E+7 (3.8×10⁷)	0.559E+7	164.0

Figure 1. Characterization of iMSCs, iAAT-MSCs, and their secreted EVs

(A) Morphology of iMSCs and iAAT-MSCs in culture under the light microscope (top, scale bar, 200 μm) and after the cells were infected with SV40LT, sorted by fluorescence-activated cell sorting, and observed under a fluorescent microscope; SV40LT is shown in red, scale bar, 100 μm. (B) Mean intensity of EV size and (C) size distribution derived from iMSCs and iAAT-MSCs measured by NTA and laser scattering microscopy. (D) The morphology of iMSC- and iAAT-MSC-EVs as observed by TEM. (E) Protein expression of CD63, CD81, CD9, and AAT in iMSC- and iAAT-MSC-EVs by western blot analysis.

identified iron deposition using Prussian blue staining on human pancreatic tissues from healthy donors or CP patients. No detectable iron deposits were found in pancreatic sections from healthy controls. In contrast, pronounced Fe^{3+} iron overload was observed in the pancreatic sections of CP patients ($p < 0.01$ vs. healthy donors) (Figures 3B and 3C). These results suggest ferroptosis may play a role in acinar cell death in CP. Similarly, dramatic iron deposition in the pancreas and elevated serum iron levels were observed in TNBS-treated mice 6 weeks post TNBS injection compared with controls (Figures 3D–3F). These findings prove increased iron deposition and potential ferroptosis in pancreatic cells in both human and mouse CP models.

Moreover, treatment with iMSC-EVs significantly reduced iron deposition in pancreatic tissues ($p < 0.05$ vs. TNBS) (Figure 3E) and lowered serum iron concentrations in CP mice 6 weeks post treatment (Figure 3F). Next, we explored the mechanistic insights of iron deposition and the protective effects of EVs. Nuclear receptor coactivator 4 (NCOA-4) is a key mediator of ferritin-selective autophagy, which increases free iron and promotes ferroptosis.[31] NCOA4 binds to ferritin heavy chain 1 (FTH1), forming an NCOA4-FTH1 complex that facilitates the delivery of iron-bound ferritin to autophagosomes for lysosomal degradation and iron release, contributing to ferroptosis.[32,33] Treatment with TNBS led to a significant upregulation of FTH1 and NCOA4 mRNA expression levels in mouse pancreatic tissue 6 weeks post treatment (Figure 3G). In contrast, the iMSC-EV group showed a trend of decrease in FTH1 and NCOA4 mRNA level compared with the TNBS group ($p < 0.05$) (Figures 3G–3I). Similarly, both iMSC and iAAT-MSC-EVs significantly reduced FTH1 protein expression compared with

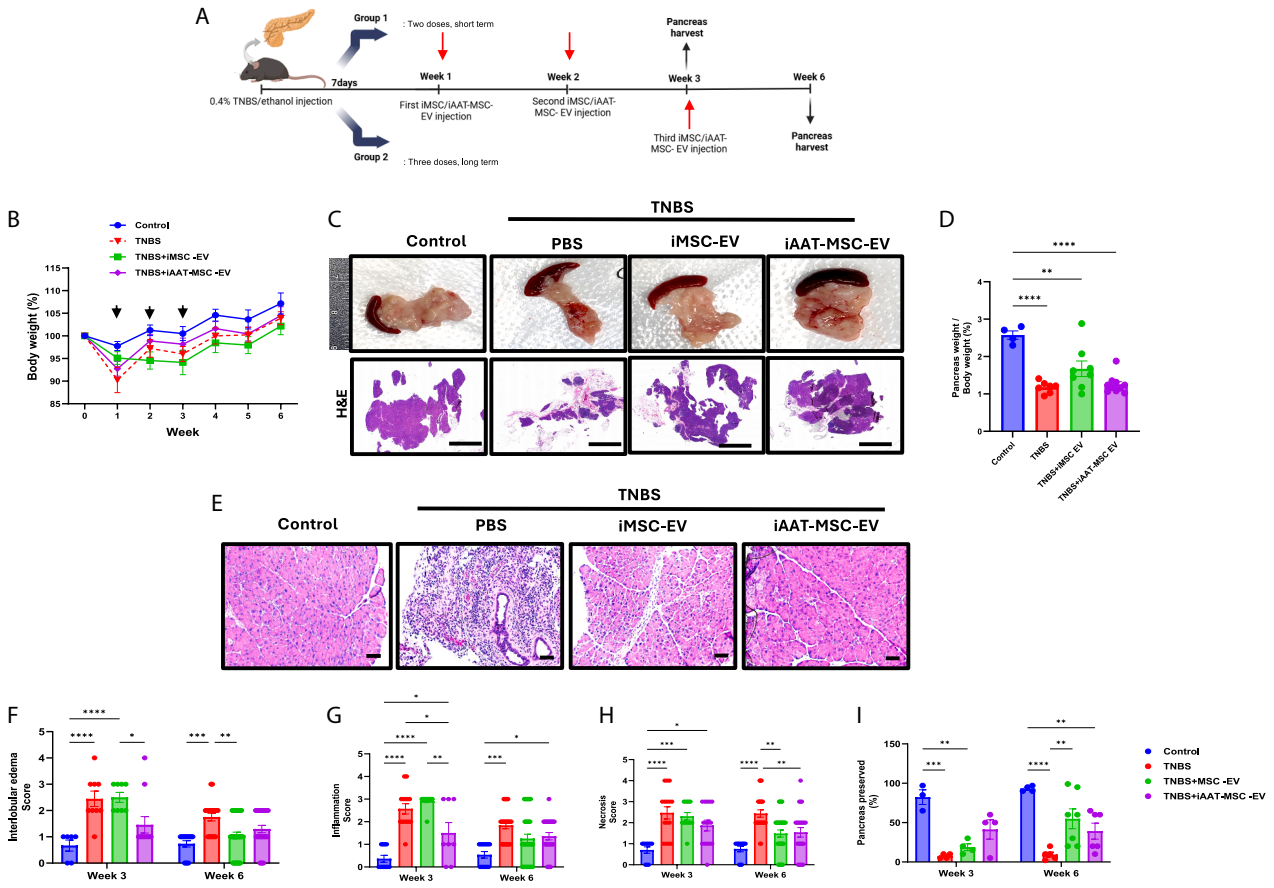

Figure 2. EV treatments preserve the pancreas from TNBS-induced damage in mice

(A) Schematic diagram of TNBS-induced CP, EV administration, and tissue collection and analysis. (B) Percentages of changes in body weight at different weeks post treatment. The arrows signify the infusion of iMSC or iAAT-MSC-EVs; $N = 5–11$ per group. (C). Images of the pancreas and spleen were collected, and H&E staining of whole pancreas sections from the control group, TNBS, and TNBS mice was treated with iMSCs or iAAT-MSCs (treatment mice) 6 weeks after TNBS infusion. Samples were collected at 6 weeks of TNBS injection. (D) Percentage change in pancreas weight relative to body weight, measured 6 weeks after TNBS infusion (E) Light microscope observations of H&E-stained pancreatic tissue sections to assess edema, inflammatory cell infiltration, and acinar necrosis in the control group, TNBS, and TNBS mice treated with iMSCs or iAAT-MSCs, 6 weeks after TNBS infusion; scale bar, 50 μm. (F–I) Scores for interlobular edema (F), inflammation (G), necrosis (H), and percent of pancreas preserved (I) evaluated by a pathologist blinded to group assignment measured at 3 and 6 weeks post TNBS treatment, $n = 3–8$ per group.
Data presented as mean ± SD. $^{*}p < 0.05$, $^{**}p < 0.01$, $^{***}p < 0.001$, $^{****}p < 0.0001$.

the TNBS group ($p < 0.05$) (Figure 3I). iAAT-MSC-EV-treated mice showed reduced expression of both FTH1 and NOCA4 at protein levels compared with the TNBS group ($p < 0.01$) (Figures 3H and 3J). These findings highlight the role of FTH1 and NCOA4 in iron metabolism and ferroptosis induced by TNBS and demonstrate the potential protective effects of iMSC and iAAT-MSC-EVs in mitigating these processes.

EV treatments enhance antioxidant pathways in the pancreas of CP mice

Nuclear factor erythroid 2-related factor 2 (NRF2) modulates the cellular ferroptosis response.[33–35] Other antioxidant systems, including GPx4 and ferroptosis suppressor protein (FSP1), are also critical in reducing lipid peroxides and protecting cells from ferroptosis.[34,36] Moreover, decreased levels of SOD can contribute to acinar cell damage, triggering inflammation, pancreatic edema, and inflammatory cell aggregation.[34] We tested whether EV treatment enhances the antioxidant pathways in the pancreas of CP mice (Figure 4A). Pancreas samples from the TNBS group showed reduced NRF2 expression compared with the control, while those from iMSC- and iAAT-MSC-EV groups exhibited a significant increase compared with the TNBS group ($p < 0.05$) (Figure 4B). Although the mRNA expression of GPx4 in the pancreas increased in the iMSC- and iAAT-MSC-EV treatment groups, the differences were not statistically significant when compared with the TNBS group ($p = 0.66$, and $p = 0.20$, respectively) (Figure 4B). Additionally, iMSCs-EV-treated mice demonstrated a significant increase in FSP1 and iAAT-MSC-EV showed increase on both FSP1 and SOD1 mRNA expression in the pancreas compared with the TNBS group (SOD1: $p < 0.01$ and FSP1: $p < 0.0001$) (Figure 4C).

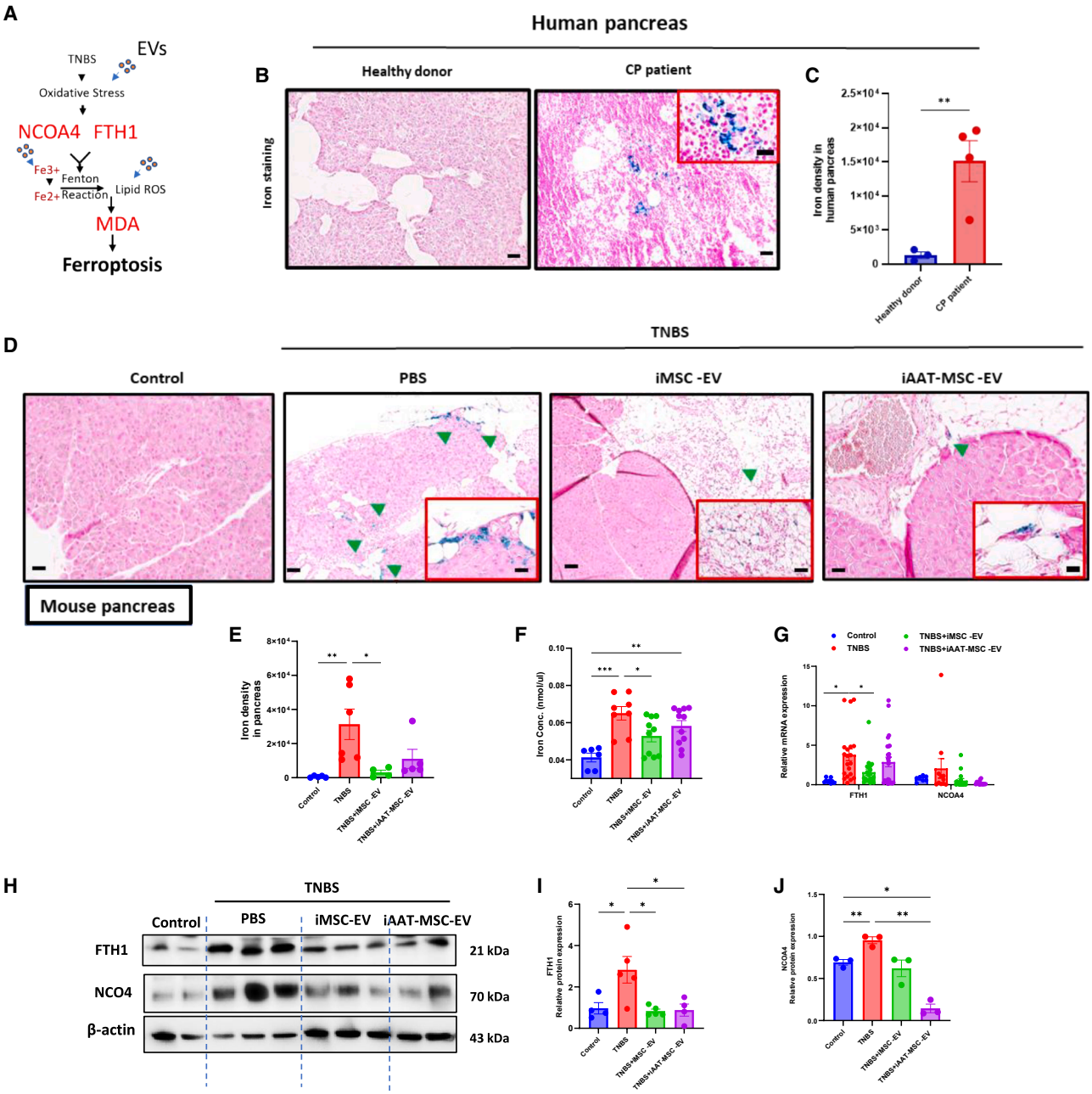

Figure 3. iAAT-MSCs-EVs mitigate ferroptosis by regulating iron metabolism pathways mediated by FTH1 and NCOA4

(A) The hypothetic pathway on how EVs suppress TNBS-induces ferroptosis. (B) Prussian blue staining demonstrated the accumulation of Fe^{3+} ions in the pancreas of CP patients but not in healthy donors; scale bars, 150 μm and 75 μm (inside the red box). (C) Quantification of iron density in human pancreas sections using ImageJ, $n = 3–4$ per group. (D) Prussian blue staining demonstrated the accumulation of $Fe3^{+}$ ions in EV-treated and untreated mice 6 weeks of TNBS injection; scale bars, 150 μm and 75 μm. (E) For the quantification of iron density from Prussian blue-stained pancreas sections using ImageJ, five randomly selected fields were analyzed for iron density, $n = 4–6$ per group. (F) Serum iron levels in mice from different groups at 6 weeks after treatment; $n = 5–11$ per group. (G) Total mRNA expression levels of FTH1 and NCOA4 in pancreas tissue in control, TNBS alone, or EVs-treated mice at 6 weeks post treatment were analyzed by RT-PCR analysis. β-actin was used as an internal control for normalization; $n = 5–11$per group. (H–J) The protein expression levels (H) and quantification of FTH1 (I) and NCOA4 (J) in pancreases were measured by western blot analysis. β-actin was used as the internal control; $n = 3–4$ per group.

Data are shown as mean ± SD. $^{*}p < 0.05$, $^{**}p < 0.01$, $^{***}p < 0.001$. All mice samples were collected 6 weeks after treatment.

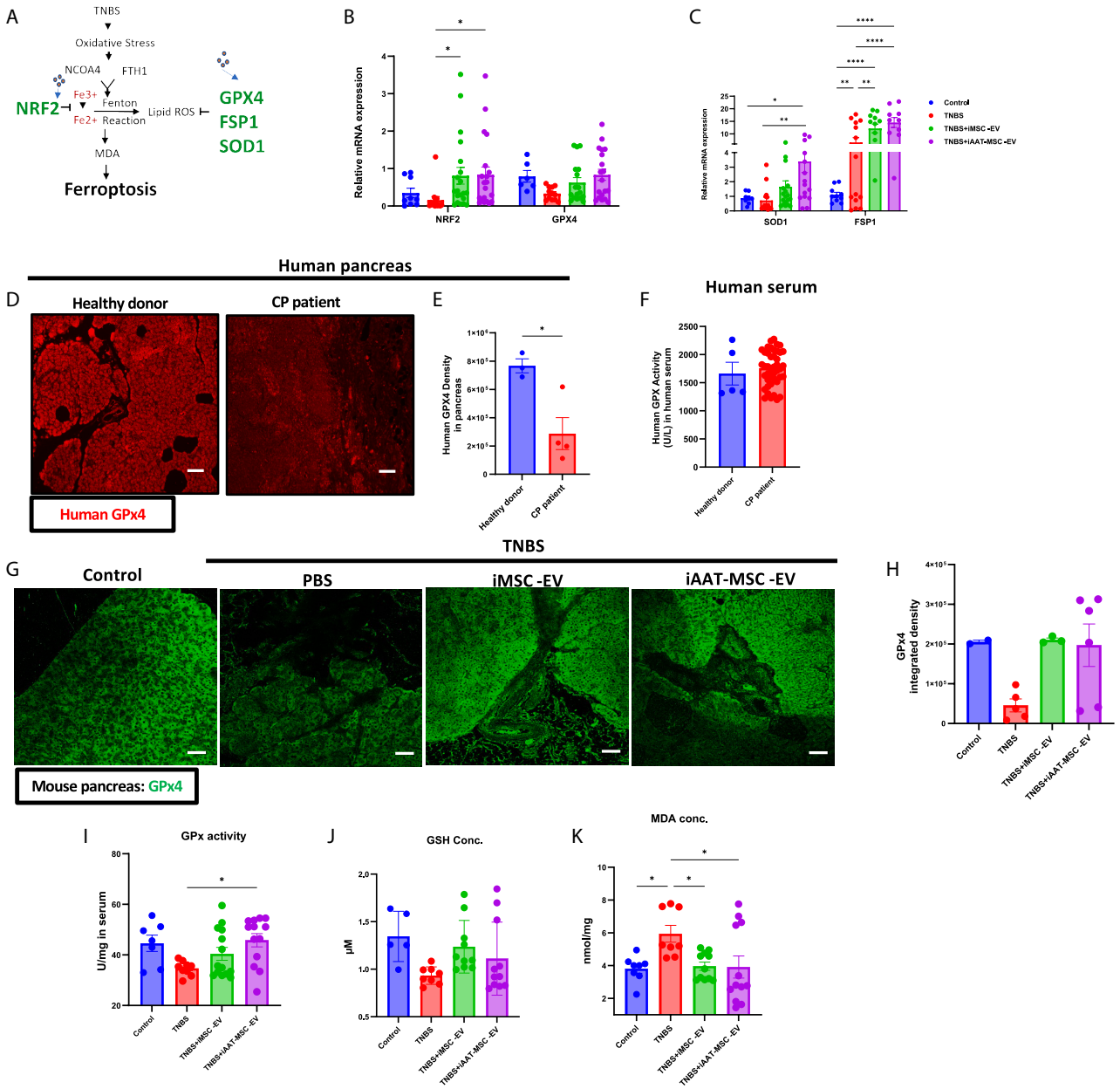

Figure 4. Reduced anti-oxidative defense in the pancreas of CP patients and mice and iAAT-MSC-EV treatment upregulating anti-oxidative pathways

(A) Schematic overview of how EVs intervene in the antioxidative pathways during TNBS-induced ferroptosis. (B and C) The total mRNA expression levels of (B) GPx4, NRF2, (C) SOD1, and FSP1 were analyzed in mouse pancreases of control, TNBS, and TNBS with EV treatment by RT-PCR after 6 weeks of TNBS injection. β-actin was used as an internal control to standardize the values; n = 5–11 with technical replicants. (D and E) Immunofluorescence staining (D) and quantification (E) of the GPx4 in human pancreas from healthy donors or CP patients, Scale bar, 150 μm. *N* = 3–4. (F) Serum GPx4 activity from healthy controls and CP patients. Each dot represents a donor. (G and H) GPx4 protein expression levels, assessed by immunofluorescent staining (G), were quantified using integrated density (H) of pancreatic sections from mice in each treatment group; *n* = 2–6 per group. (I) GPx activity was measured in control and CP mice treated with PBS or EVs. (J) GSH levels were analyzed in serum samples of control and three TNBS-treated groups, 6 weeks after TNBS injection, *n* = 5–11 per group. (K) Level of MDA in the pancreases of mice from four groups of mice after 6 weeks of TNBS injection, *n* = 5–11 per group.

Data are shown as mean ± SD. $^{*}p < 0.05$, $^{**}p < 0.01$, $^{***}p < 0.001$, $^{****}p < 0.0001$.

Decreased GPx4 activity or level is often considered a hallmark of ferroptosis.[33,37] We continued our assessment by analyzing GPx4 protein expression and activity in pancreatic samples from both humans and CP mice. Immunostaining unveiled a reduction in GPx4 expression in pancreatic acini among CP patients compared with healthy individuals ($p < 0.05$) (Figures 4D and 4E). However, no significant difference in GPx4 activity was observed in serum samples from healthy donors or CP patients (Figure 4F). In the pancreas of CP mice, the immunofluorescence assay for GPx4 demonstrated lower GPx4 density compared with controls. Treatment with EVs resulted in an elevated density of GPx4 expression and increased serum GPx4 activity (Figures 4G–4I). Notably, iAAT-MSC-EV-treated mice exhibited significantly increased GPx4 activity compared with TNBS-treated mice ($p < 0.05$) (Figure 4I). These data indicate that EV treatment restored the antioxidant capacity of pancreatic cells.

Biological traits related to cell ferroptosis mainly include impaired metabolism of iron ions, depletion of glutathione (GSH), and the presence of harmful byproducts like malondialdehyde (MDA) and 4-hydroxynonenal resulting from the breakdown of lipid peroxides.[33,37] In the context of EV treatment, the groups receiving EVs displayed a trend of restored serum GSH concentrations like those of sham controls (Figure 4J). Intriguingly, both EV-treated groups demonstrated significantly lower levels of pancreatic MDA compared with the TNBS group ($p < 0.05$) (Figure 4K). Taken together; these data suggest the presence of ferroptosis in both human and mouse CP conditions and treatment with iMSC- or iAAT-MSC-EVs seems to mitigate ferroptosis by reducing the presence of factors that contribute to this process, while simultaneously enhancing anti-oxidative responses in CP mice.

EVs derived from iAAT-MSCs mitigate pancreatic fibrosis

Another typical feature of CP is pancreatic fibrosis, mainly arising from excessive production of extracellular matrix proteins from PSCs. This process consequently leads to acinar cell injury (Figure 5A).[38] Upregulation of α-smooth muscle actin (α-SMA), a marker of fibrosis secreted by PSCs,[39] was evident in the pancreas of CP patients compared with healthy donor pancreases ($p < 0.05$) (Figures 5B and 5C). Additionally, there was a significant increase in amylase activity in CP patients ($p < 0.05$ vs. healthy donors) (Figure S2A), suggesting acinar cell damage occurred.

Like human samples, significant upregulation of α-SMA was also observed in CP mice compared with the control mice ($p < 0.05$) (Figures S2B and S2C). Furthermore, CP mice exhibited notable pancreatic atrophy and widespread intralobular fibrosis compared with controls, as evidenced by Masson's trichrome staining of the whole pancreas and the fibrosis score (week 3: $p < 0.0001$, and week 6: $p < 0.01$ vs. control) (Figures 5D and 5E). In contrast, mice treated with iAAT-MSC-EVs demonstrated preserved pancreatic parenchymal and significantly diminished fibrosis 3 weeks post treatment (Figures 5D and 5E). The western blot analysis demonstrated upregulation of transforming growth factor β1 (TGF-β1) and matrix metalloproteinase 2 (MMP2), both known proinflammatory cytokines implicated in tissue fibrosis[38,40] in mice treated with TNBS (Figures 5F and 5G). EV treatments led to a significant reduction in the expression of TGF-β1 and MMP2, suggesting suppression of fibrosis-related pathways following EV therapy (iMSC-EV, $p < 0.001$ for both proteins; iAAT-MSC-EV, $p < 0.01$ for TGF-β1; and $p < 0.05$ for MMP2 compared with TNBS) (Figures 5F and 5G).

iAAT-MSC-EVs alleviate pain associated with CP and suppress macrophage infiltration into the pancreas

Subsequently, we evaluated the effect of EVs on TNBS-induced pain, another prominent feature of CP. We used the open-field test to assess hyperactivity and anxiety levels in our mouse models, by measuring the duration and distance traveled within the central area of the maze.[41] At 6 weeks after treatment, TNBS-treated mice exhibited a significant increase in the time spent in the center (Figure S3A), higher velocity, greater distance covered within the center, and more frequent entries into the center compared with the control mice (Figures S3B–S3D). In contrast, mice treated with iMSC-EVs exhibited lower velocity, traveled shorter distances, and made fewer entries into the center than TNBS mice at week 6 (velocity and distance, $p < 0.01$; and entrance, $p < 0.05$ vs. TNBS) (Figures S3B–S3D), aligning more closely with the behavior of sham controls.

Furthermore, TNBS mice demonstrated a substantially increased threshold in paw withdrawal and abdominal sensitivity throughout the experiment compared with the healthy controls, as measured at weeks 3, 5, and 6 (Figures 6A and 6B). Both iMSC- and iAAT-MSC-EV treatments alleviated the sensitivity to these stimuli in TNBS mice at weeks 5 and 6, with iAAT-MSC-EVs demonstrating greater improvement.

The damage to pancreatic acinar cells results in the infiltration of macrophages that can exacerbate inflammation in the pancreas[28,42] (Figure 6C). We observed significantly higher infiltration of $CD68^+$ macrophages in the pancreas from CP patients compared with healthy individuals ($p < 0.05$) (Figures 6D and 6E). Moreover, the expression of inducible nitric oxide synthase (iNOS) and interleukin (IL)-10 proteins, markers of M1 and M2 macrophages, respectively, were higher in pancreases from CP patients than those from healthy donors (iNOS, $p < 0.01$) (Figures S3E and S3F). Similarly, the presence of $CD68^+$ macrophages was also observed in the pancreas samples of TNBS-treated mice (Figure 6F). Again, both EV treatment groups exhibited significantly lower protein density in CD68 compared with the TNBS group ($p < 0.001$, iMSC-EV vs. TNBS, and $p < 0.01$, iAAT-MSC-EV vs. TNBS) (Figure 6G). Furthermore, the iAAT-MSC-EV group demonstrated significant suppression of M1 macrophage-related gene expression (CD11c, $p < 0.05$ vs. TNBS) (Figure S3G) and an increase in M2 macrophage-related gene expression (CD206) compared with the TNBS group (Figure S3H). Additionally, the iMSC- and iAAT-MSC-EV groups showed significantly lower protein expression of CD11c compared with the TNBS-treated group, while both exhibited substantially higher protein expression of CD206 compared with the TNBS group

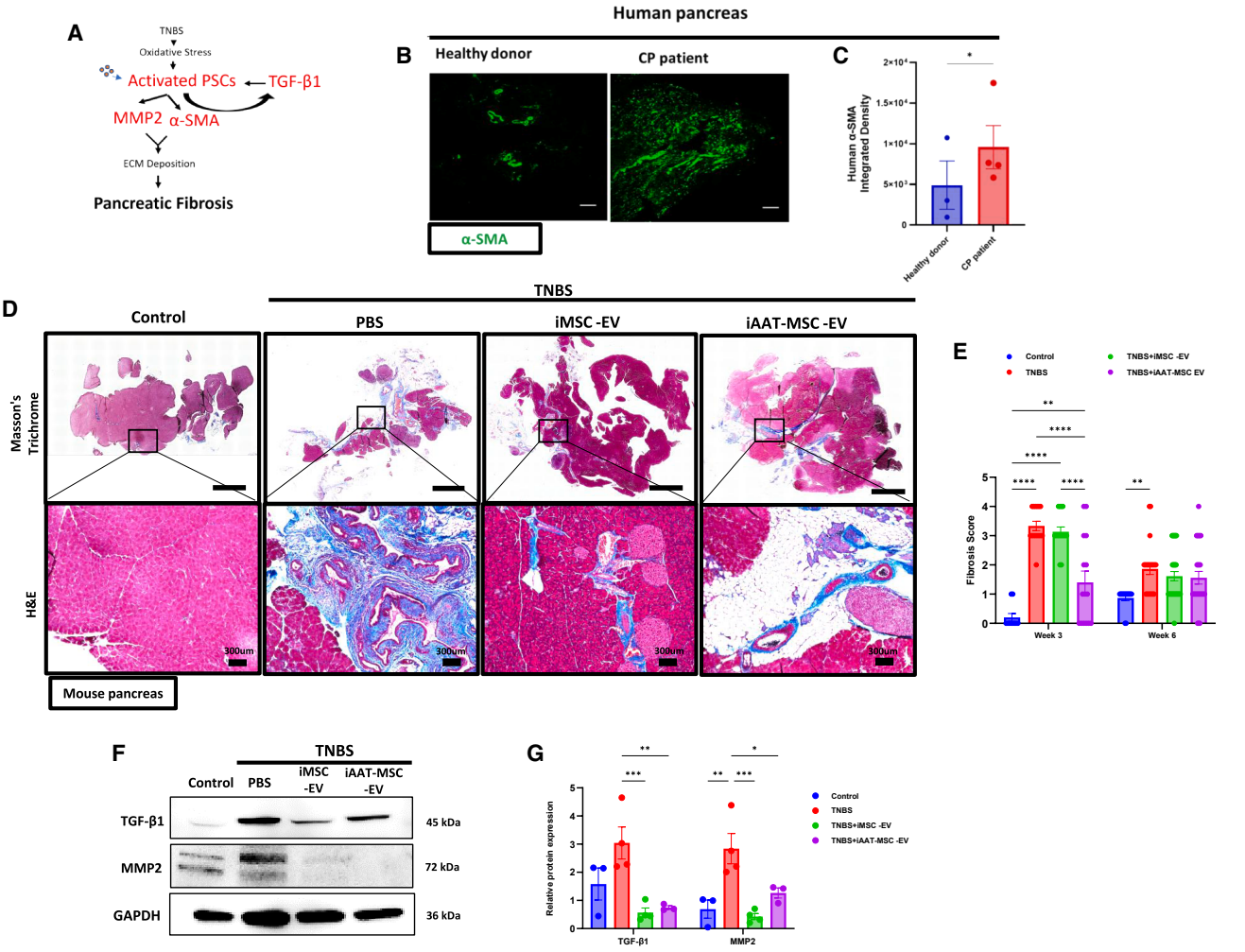

Figure 5. EV treatment reduces fibrosis associated with CP

(A) The hypothetic pathway on how EV suppresses TNBS-induced pancreatic fibrosis. (B) The expression levels of α-SMA, a marker for fibrosis, were evaluated in pancreatic tissue sections obtained from healthy individuals and CP patients; Scale bar, 150 μm. (C) The integrated density analysis revealed a significant increase in α-SMA expression in the pancreas of patients diagnosed with CP; $n = 3–4$. (D) Masson trichrome staining shows fibrosis in the control, TNBS only, and TNBS with EV groups, 6 weeks of TNBS injection: Scale bar, 2 mm or 300 μm (enlarged photos). (E) Fibrosis score obtained by a blinded pathologist in pancreas tissues from control, TNBS alone, or TNBS plus EV groups at 3 and 6 weeks of TNBS injections. (F) Protein expression of TGF-β1 and MMP2, and (G) Quantification of TGF-β1 and MMP2 in the pancreas was analyzed by western blot in the control, TNBS, iMSCs-EV, and iAAT-MSC-EV groups at week 6. GAPDH was used as the loading control; $n = 3–4$ per group.
Data are presented as mean ± SD. *$p < 0.05$, **$p < 0.01$, ***$p < 0.001$, ****$p < 0.0001$. ECM, extracellular matrix.

(iMSC-EVs, $p < 0.05$ and iAAT-MSC-EVs, $p < 0.01$) (Figures S3I and S3J).

Moreover, in the dorsal root ganglia (DRG), CD68 expression was significantly higher in TNBS-treated mice than in controls ($p < 0.0001$) (Figures S4A and S4B). Intriguingly, both EV treatment groups exhibited reduced fluorescence density in CD68 staining compared with the TNBS group ($p < 0.0001$), indicating that EV treatment effectively mitigated TNBS-induced macrophage infiltration in both the pancreas and the DRG. This reduction in macrophage infiltration may have contributed to the observed decrease in inflammation.

EV therapy inhibits mast cell infiltration and reduces iron channel protein expression

In addition to monocytes, mast cells are a secondary innate immune cell type within the pancreas, their activation can mediate neuropathic pain in acute and chronic pancreatitis[28,43,44] (Figure 7A). We observed a greater abundance of mast cells in the pancreas of CP patients compared with those from normal individuals ($p < 0.05$) (Figures 7B and 7C). This finding was further validated in CP mice. When comparing mast cell density in the pancreas and DRG, TNBS mice exhibited significantly higher mast cell density in both tissues compared with the control group at six weeks after TNBS injection ($p < 0.0001$ TNBS vs. control in pancreas and

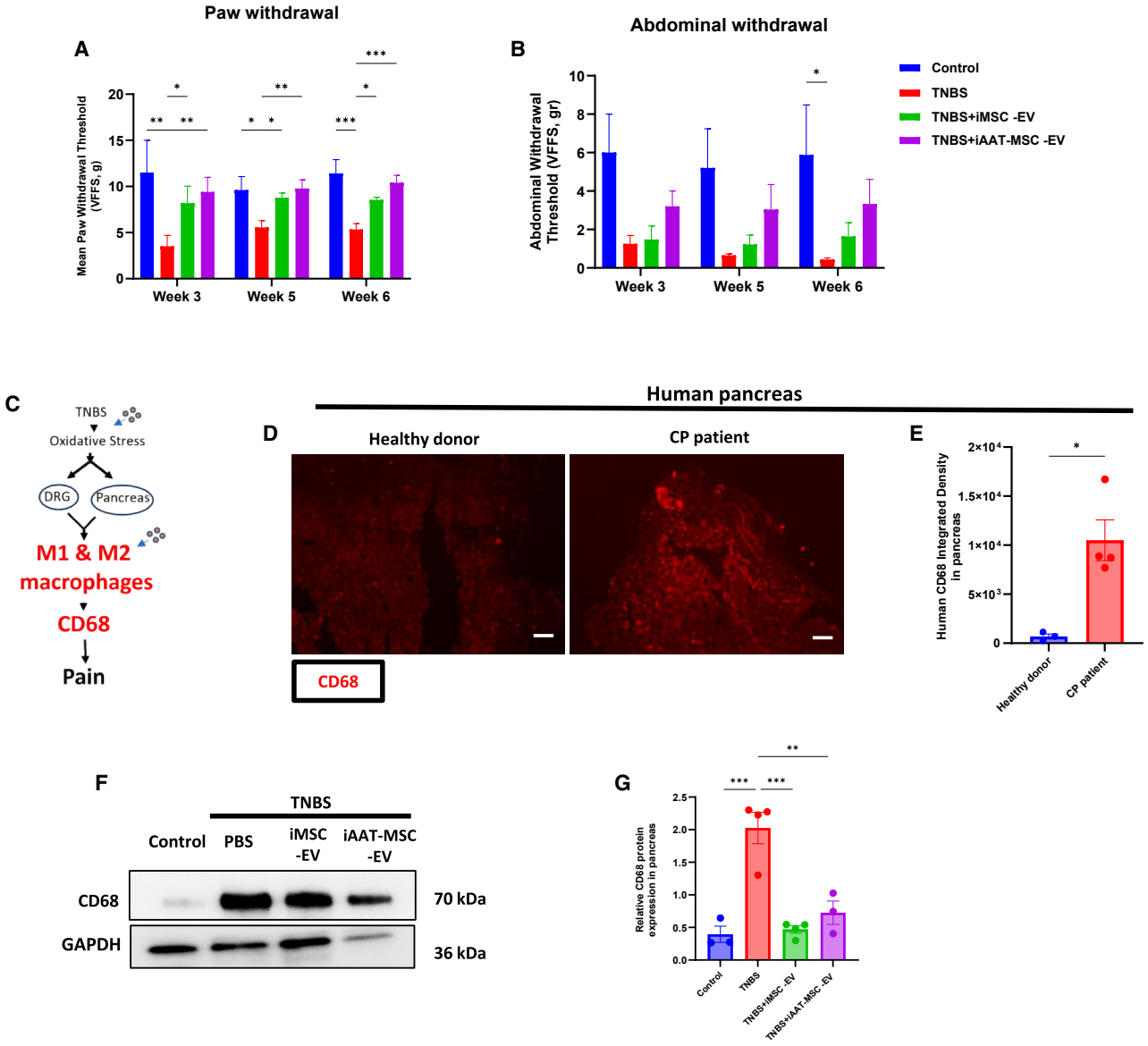

Figure 6. iMSC- and iAAT-MSC-EVs alleviated CP pain and reduced macrophage infiltration

(A and B) Mechanical sensitivity was assessed using calibrated VFFs with a 0.40–15 g range. Mice were tested for sensitivity on the hind paw (B) and abdomen (C) at 3, 5, and 6 weeks following TNBS injection. N = 5–11 per group. (C) The proposed pathway through which TNBS induces pancreatic and DRG pain. (D and E) The presence (D) and intensity (E) of $CD68^+$ macrophages evaluated in pancreatic tissue sections from healthy donors and CP patients; scale bar, 150 μm; N = 3–4. (F and G) CD68 protein expression was measured using western blot (F) and quantification (G) in the control, TNBS, iMSCs-EV, and iAAT-MSC-EV groups after 6 weeks of TNBS injection. GAPDH was used as the loading control. n = 3–4 per group.

Data are shown as mean ± SD. *p < 0.05, **p < 0.01, ***p < 0.001, ****p < 0.0001. VFFs, von Frey filaments.

p < 0.01 TNBS vs. control in DRG) (Figures 7D–7F). Moreover, mice treated with iMSC- and iAAT-MSC-EVs showed significantly fewer mast cells in the pancreas than TNBS mice (p < 0.001 and p < 0.0001, respectively) (Figures 7D and 7E). Additionally, iMSC- and iAAT-MSC-EVs exhibited lower mast cell density in the T9-T12 DRG, with the difference being significant for iAAT-MSC-EVs compared with the TNBS group (p < 0.05) (Figures 7D and 7F). These findings suggest that EVs alleviate pain by inhibiting mast cell migration to the pancreas and the DRG.

EV treatments reduce the expression of pain markers in the DRG

Neurogenic inflammation plays a pivotal role in pain-related behaviors in CP. Sensory nerves are associated with neurogenic inflammation and house the cell bodies of these nerves in the DRG.[28,45] In the

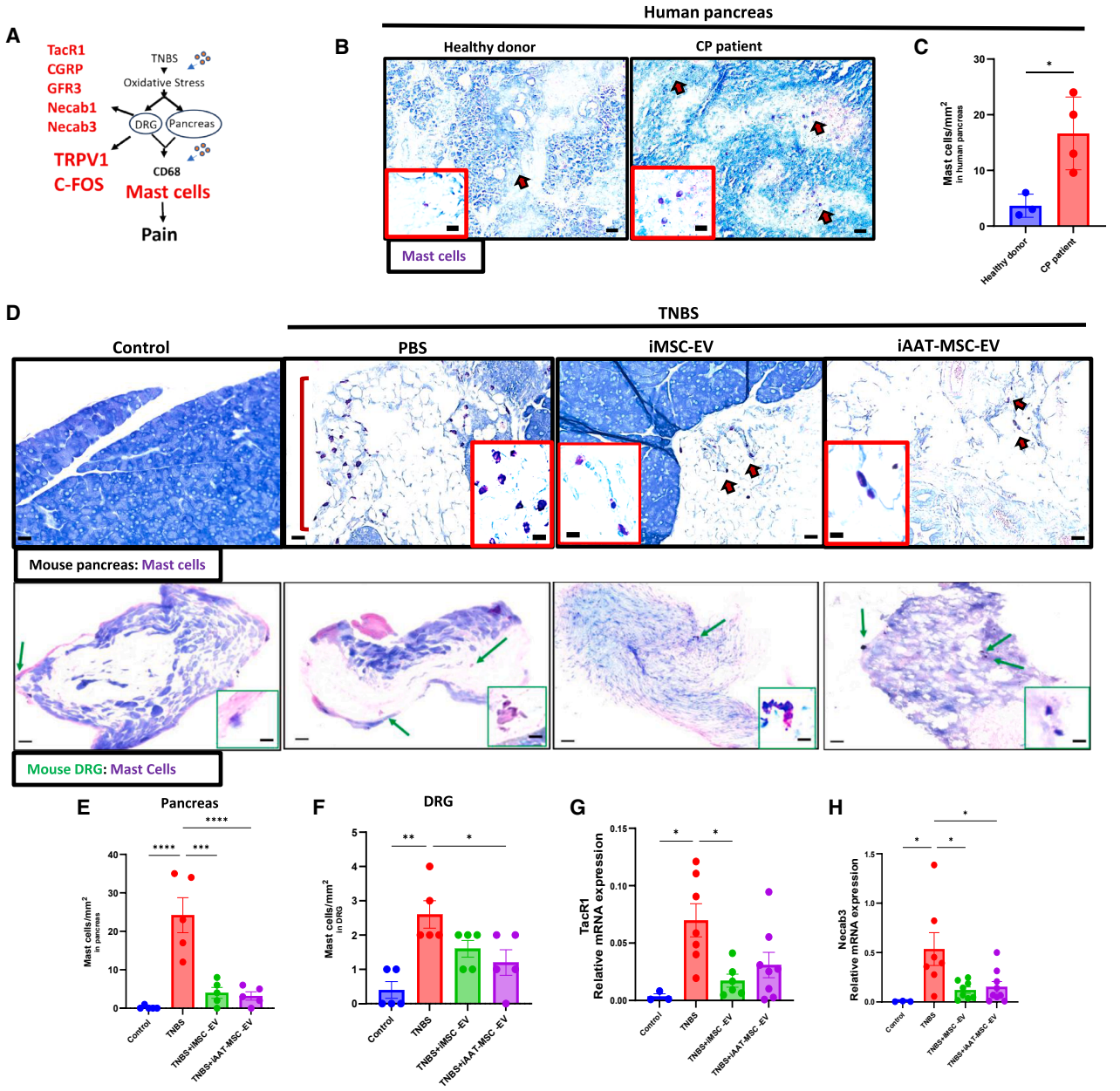

Figure 7. iMSC- and iAAT-MSC-EVs reduce mast cell intensity and the expression of pain markers TacR1 and Necab3

(A) Illustration of potential interactions between EVs and pain mediators. (B) Presence of mast cells in the pancreas from healthy donors or CP patients. Yellow arrows point to mast cells. Scale bar, 150 μm and 75 μm (inner box). (C) Pancreas sections from CP patients showed an elevated mast cell density; $n = 3–4$. (D and F) Presence of mast cells and mast cells/mm^2 in the pancreatic (top, D and E) and DRG sections (bottom, D and F) from the sham control, TNBS, TNBS treated with EVs. Red arrows indicate mast cells in the pancreas. Green arrows indicate mast cells in the DRG. Scale bar, 75 μm and 50 μm (inner box); $n = 4–5$ per group. mRNA expression of (G) TacR1 (H) and Necab3 in control and TNBS mice receiving different treatments.

Data are shown as mean ± SD. *$p < 0.05$, **$p < 0.01$, ***$p < 0.001$, ****$p < 0.0001$. Necab3, N-terminal EF-hand calcium-binding protein 3.

DRG, various pain markers, such as the transient receptor potential ankyrin 1,[28] c-FOS,[46] tachykinin receptor 1 (TacR1),[47] neuropeptide calcitonin gene-related peptide (CGRP),[45] neuronal calcium-binding protein (Necab) family,[48] and others, have been found to increase in numerous pain models (Figure 7A). In this study, immunofluorescence staining revealed a significant increase in neuronal TRPV1 expression in TNBS-treated mice compared with controls ($p < 0.01$) (Figures S4C and S4D), consistent with previous

findings.[27,28] In contrast, EV treatment significantly reduced TRPV1 expression in TNBS mice in the iMSC-EV group, as evidenced by immunofluorescent staining ($p < 0.01$) (Figures S4C and S4D). Additionally, the iAAT-MSC-EV-treated group displayed a non-significant decrease in c-FOS, resembling the levels in the sham control group (Figures S4C and S4D). Notably, iMSC-EV treatments resulted in a significant reduction of TacR1 mRNA expression, akin to the control group, compared with TNBS-treated DRG ($p < 0.05$) (Figure 7G), while the pain markers CGRP, fibroblast growth factor receptor and Necab1, exhibited lower mRNA expression in the EV treatment groups (Figures S4E–S4G). The reduction in Necab3 expression was significant in the treatment groups compared with the TNBS group ($p < 0.05$) (Figure 7H). Overall, both EV treatment groups demonstrated amelioration in CP pain, as evidenced by reduced pain marker expression and decreased infiltration of macrophages and mast cells.

DISCUSSION

This study shows compelling evidence of iron deposition/ferroptosis, fibrosis, macrophage, and mast cell infiltration within the pancreas of patients with CP, mirroring observations in a murine model of CP induced by TNBS. Our results underscore the presence of oxidative stress and pancreatic cell ferroptosis that is not balanced by adequate anti-oxidative protection in the TNBS-induced mouse model of CP. Additionally, EVs derived from iAAT-MSCs or iMSCs suppressed ferroptosis pathways, sustained GPx4 activity, and attenuated fibrosis in the damaged pancreas. Moreover, EV treatment alleviated pain, likely by preventing macrophage and mast cell infiltration into the pancreas and/or the DRG. These findings provide valuable insights into how iAAT-MSCs-derived EVs contribute to pancreatic repair, thereby advancing the development of a cell-free therapy for CP. Compared with cell therapy, EVs may offer advantages such as their inability to mutate and the ease of administration. These attributes make EVs a potential therapeutic option and delivery tool.[49–51] Understanding the therapeutic effects of EVs and the mechanistic insights can help to optimize treatment strategies for CP.

We also found that iAAT-MSC-EVs were superior to iMSC-EVs in the majority of assays performed. This was the hypothesis in the construction of this therapeutics since AAT is a broad multifunctional anti-protease with additional anti-inflammatory functions. The superior functions of iAAT-MSC-EVs included preservation of pancreatic tissue, prevention of edema and fibrosis, and suppression of inflammation and ferroptosis. The exception was that iMSC-EVs seemed to be more effective in reducing pain markers such as TACR1. In our previous work on CP using AAT-MSCs and MSCs, TRPV1 was significantly reduced in mice treated with either cell type.[28]

Ferroptosis was evident in human pancreatic tissues from CP patients. Similarly, both mRNA and protein levels of oxidative stress-related genes were significantly elevated, and anti-oxidative genes were downregulated in TNBS-induced CP mice. These results indicate that TNBS-induced pancreatitis involves iron accumulation, lipid peroxidation, and impairment of redox homeostasis, all of which are essential characteristics of ferroptosis, indicating the involvement of ferroptosis in TNBS-induced CP in mice. Research by Xu et al.[52] demonstrated increased iron overload and elevated levels of MDA and FTH1, which decreased following ferrostatin-1 treatment in colitis. Notably, anti-ferroptosis markers FSP-1, SOD1, GPx4, and NRF2 were decreased in CP mice, consistent with findings from studies on diabetic conditions and pancreatic adenocarcinoma.[36,53,54] Other studies demonstrated that treatment with anti-ferroptosis drugs could increase GPx4 levels in osteoarthritis and CP.[13,55] In line with these findings, our study introduces a novel therapeutic avenue by utilizing EV treatment derived from iMSCs or iAAT-MSCs to mitigate CP in mice, restoring redox homeostasis and reducing the expression of iron-dependent genes.

Other mechanisms of cellular injury, senescence, and death are undoubtedly present in the complicated models of CP. One pathway by which therapy may be helpful is through induction of the PI3K/Akt pathway by iAAT-MSC-EVs. This pathway plays a crucial role in MSCs, regulating processes such as survival, proliferation, migration, differentiation, and angiogenesis. It supports cell viability by upregulating anti-apoptotic proteins such as Bcl-2 and downregulating pro-apoptotic proteins like Bax. The PI3K/Akt pathway also drives MSC proliferation through beta-catenin, facilitates migration by modulating cytoskeletal dynamics, and enhances angiogenesis by stimulating VEGF secretion.[56,57] By transferring the benefits of this pathway to recipient cells, iAAT-MSC-EVs may enhance regenerative and immunomodulatory responses.

Additionally, treatment with EVs also resulted in a reduction in α-SMA-positive cells, along with a decreased expression of MMP2 and TGF-β1 compared with TNBS mice. This finding suggests that EVs have the potential to hinder pancreatic fibrosis by suppressing the activation of PSCs,[39] regulating the secretion of extracellular matrix, and cell death.[38] Furthermore, the decreased presence of $CD68^+$ macrophages indicates alterations in the immune microenvironment and neuropathological conditions, aligning with findings reported in other studies.[42,58]

Another potential mechanism by which iAAT-MSC-EVs preserved pancreatic tissue is through effects on miRNAs. Notably, the increased expression of anti-ferroptosis miRNAs such as miR-9-5p and miR-10a-5p in iAAT-MSC-EVs, suggests their enhanced ability to suppress lipid ROS accumulation and maintain iron homeostasis.[59,60] Upregulation of miR-10a-5p may further reduce IL-6 receptor levels, mitigating IL-6-associated ferroptosis.[60] Furthermore, miR-21-5p and miR-660-5p were downregulated in iAAT-MSC-EVs compared with iMSC-EVs, which might have contributed to their differences in regulating the ferroptosis process.[61,62] Additionally, the EVs carried some specific miRNAs, such as those from the miR-200 family and miR-92a in iAAT-MSC-EVs, as well as miR-29 in iMSC-EVs, that mitigate TGF-β1-induced expression and α-SMA in fibrotic phenotypes.[63]

Macrophage polarization was affected by exposure to the EV preparations. Macrophages may play a vital role in pancreatic repair and regeneration.[64] Pancreatic acinar cells conversely regulate macrophage activation by secreting EVs carrying specific miRNAs. This complex interaction between native pancreatic cells, macrophage subpopulations, and the EVs given will require dedicated studies that target genes of differentially expressed miRNAs and macrophage activation, likely via the TRAF6-TAB2-TAK1-NIK/IKK-nuclear factor κB (NF-κB) pathway.

Mast cell activation and visceral pain are linked to conditions such as complex regional pain syndromes, pancreatic cancer, and CP.[28,44,65] A significant increase in mast cell presence was observed in pancreatic and DRG tissues from CP mice, suggesting a potential role for these cells in the pathogenesis of pain. This aligns with observations in CP patients, where heightened mast cell density was observed, consistent with reported study.[44] Remarkably, EV treatment in CP mice reduced mast cell numbers and decreased the expression of pain markers, including TRPV1, TacR1, and Necab3, in the DRG. This indicates that both iMSC- and iAAT-MSC-EVs act peripherally to restore neuroplasticity in CP mice. These findings are consistent with previous research suggesting that increased synthesis of pain peptides in the DRG may contribute to the pathogenesis of chronic inflammatory pain.[45] One potential factor in EVs impacting these findings is miR-146a, an immune system regulator, that modulates NF-κB activation, T regulatory cell function, and mast cell degranulation.[63,66] miR-146a was significantly expressed in EVs from iAAT-MSCs, highlighting their immunomodulatory potential.

Both iMSC- and iAAT-MSC-EVs exhibit effectiveness in suppressing CP pathology, albeit to varying degrees, likely attributed to their specific miRNA cargo. For instance, EVs derived from both cell types identified essential miRNAs, such as those belonging to the let-7 family, miR-375, and miR-455-3p. These miRNAs play critical roles in maintaining normal pancreatic function and mitigating injury to pancreatic acinar cells.[67–70] Additionally, miR-144-3p in both types of EVs suggests their potential to suppress ferroptosis and pancreatic β-cell dysfunction.[71]

Recent clinical trials have demonstrated the significant therapeutic potential of EVs including exosomes derived from MSCs across various diseases.[72–74] For instance, in coronavirus disease 2019 (COVID-19), EVs from unspecified MSC sources have been evaluated for their potential to treat pneumonia and acute respiratory distress syndrome (NCT04798716). Similarly, another study targeting hyper-inflammation in moderate COVID-19 patients administered EVs intravenously on days 1 and 7, highlighting their role in immune modulation (NCT05216562). Beyond respiratory applications, MSC-derived EVs have been explored in regenerative medicine.[72] For example, umbilical cord MSC exosomes were utilized to promote the healing of large and refractory macular holes by direct delivery into the vitreous cavity after surgery (NCT03437759). The application of MSC-derived EVs has also extended to fibrotic and inflammatory disorders.[72,74] These trials collectively highlight the versatility and therapeutic promise of MSC-derived EVs in modulating inflammation, promoting angiogenesis, and addressing tissue fibrosis. Their application in CP, a condition characterized by inflammation and fibrosis, aligns well with these mechanisms. Leveraging EV-based therapies could open new avenues for managing disease progression and enhancing pancreatic tissue repair, reinforcing the need for further research and clinical translation.

There are some limitations to our study. Our EV subtype used may be method-specific with heterogeneity of vesicle populations within the isolated preparations.[75] Most published clinical trials used the ultracentrifugation method or the tangential flow filtration system to concentrate condition medium and purify EVs based on vesicle sizes.[76] The use of human MSCs in mice, while common in MSC research, may only partially replicate the biological signals present in human scenarios. This could affect the generalizability of our findings and may not fully account for potential variations among donors. To improve the reliability and validity of our results, future studies should involve a larger donor pool and include a validation cohort to comprehensively understand specific changes in EV proteins and their therapeutic effects. Furthermore, our focus was on the overall impact of EVs on three typical features of CP, rather than delving into the precise molecular mechanisms by which EVs reach target tissue and exert these effects at a cellular level. We did not explore alternative methods of cellular senescence and death. Only male mice were used in the study to maintain consistency with previously published studies. Both male and female mice will be applied in future studies to better understand sex-specific differences in CP and the treatment efficacy.

The observed benefits are intrinsic to MSC properties and not influenced by the immortalization process In our recently published paper, we compared naive MSCs, naive AAT-MSCs, immortal MSC, and immortal AAT-MSCs; we found that MSCs and iAAT-MSCs possess all the key characteristics and protective functions of naive MSCs and naive AAT-MSCs.[77] As for EVs derived from MSCs, several publications demonstrate the immortalization process, either using SV40 or hTRET, does not change EV characterization or the protective effects of EVs in different cell types and disease models. For example, a recent publication by Tong et al.[78] compared immortalized placental chorionic MSCs that surpass the growth limitations of primary passage cells while retaining phenotypic characteristics and differentiation potential, and they show that the immortalization process preserves the particle size, quantity, and surface marker profiles of EVs, providing a possible approach to produce high-yield EVs suitable for disease diagnosis and treatment. These results indicate that immortalizing MSCs by the SV40LT gene does not have a major effect on their secretion of EVs and exosomes, and therefore, MSCs can be used as a high-quality single-cell source for the production of EVs. In another study, it was shown that the immortalization by hTERT expression did not affect size, number, cargo composition, or biological activity regarding anti-inflammatory, anti-fibrotic, and wound healing properties *in vitro*.[79] A similar conclusion has been obtained in hTERT-treated deer antler stem cells,[80] and in retinal epithelial cells.[79]

In summary, our study validated the presence of iron deposition, fibrosis, and immune cell accumulation in the pancreases of CP patients. We showed the efficacy of iAAT-MSC-EV treatment in alleviating typical CP symptoms. These results suggest that EVs derived from iMSCs or iAAT-MSCs harbor specific miRNAs with significant therapeutic promise, targeting the underlying mechanisms of ferroptosis, fibrosis, and pain in CP. Consequently, they represent a promising approach for CP therapy.

MATERIALS AND METHODS

Human iMSC- and iAAT-MSC culture

Human AAT-MSCs were generated by transducing human bone marrow-derived MSCs from a healthy African American male with the lentiviral vector, as previously described.[24] The transduction process involved transfecting the MSCs with the viruses for 16 h. Cells expressing GFP were sorted using fluorescence-activated cell sorting after 96 h of viral infection. MSCs transfected with empty vectors were used as MSC controls. To generate immortalized cells, the MSCs or AAT-MSCs were further transduced with SV40LT viral supernatant and subsequently selected using puromycin.[77] Clones were expanded to establish stable cell lines for further experiments. iMSCs and iAAT-MSCs between passages 18 and 20 were used in this study.

EV isolation and characterization

iMSCs or iAAT-MSCs at 70%–80% confluences were cultured in the serum-free StemPro MSC SFM medium (Thermo Fisher Scientific). After 48 h, the cell culture medium was collected, and EVs were harvested using the Total Exosome Isolation kit (Thermo Fisher Scientific). In brief, the medium was centrifuged at 2,000×*g* for 30 min to remove cells and debris before adding the total exosome isolation reagent. EVs were then harvested by ultracentrifugation at 10,000×*g* for 1 h at 4°C. The resulting pellet was washed and resuspended in an appropriate volume of PBS. Nanoparticle tracking analysis (NTA) was performed to analyze the particle size, and video images of the EVs were captured using the ZetaView BASIC NTA system (Particle Metrix).

TEM imaging

EV samples were prepared using negative staining. A 5-μL drop of the sample was placed on a glow-discharged 400-mesh carbon-coated copper grid (Carbon film 400 mesh Copper grids, Electron Microscopy Sciences, Biotrend). The sample was allowed to adhere for 30–60 s, and excess liquid was removed by touching the edge of the grid with a filter paper wedge. The grid was then stained with a 5- to 10-μL drop of freshly prepared 1% uranyl acetate in deionized water for 30–60 s. Excess stain was wicked away using a filter paper wedge, and the grid was left to air dry before imaging. Prepared grids were examined using a HITACHI H-7650 TEM (Hitachi High-Technologies Corp.).

Small RNA library construction, sequencing, and data processing

EV samples were subjected to RNA extraction to generate libraries of small RNA molecules using the exoRNeasy Maxi Kit (Qiagen). The quality and integrity of the RNA samples were assessed using a NanoPhotometer spectrophotometer (IMPLEN), Qubit RNA Assay Kit with a Qubit 2.0 Fluorometer (Thermo Fisher Scientific), and Bioanalyzer 2100 system (Agilent Technologies). Only high-quality RNA samples were utilized to construct the sequencing libraries. Novogene Corporation performed the RNA sequencing. For constructing mRNA and circRNA libraries, 5 μg of RNA per sample was employed as input material. The library preparation process involved the ligation of 3′ and 5’ adaptors to the respective ends of small RNA molecules. The resulting double-stranded cDNA libraries were enriched through PCR. Following purification and size selection, libraries with insert sizes ranging from 18 to 40 bp were prepared for sequencing on the Illumina platform with SE50 sequencing.

After sequencing, raw data underwent filtration to obtain clean reads. The small RNA tags obtained from the EV samples were aligned to the assembled genome using Bowtie.[81] These aligned tags were then compared against the miRBase 20.0 database to identify known miRNAs. Modified mirdeep2 and srna-tools-cli software were employed to determine potential miRNAs and secondary structures.[82] To predict novel miRNAs, miREvo[83] and mirdeep2[82] were utilized, considering the distinctive hairpin structure of miRNA precursors. The presence of miRNA families was investigated using the Rfam database. Target genes for the identified miRNAs were predicted using miRanda software.[84] The expression levels of miRNAs were estimated using transcripts per million.[85] Differential expression analysis was performed to identify significantly differentially expressed miRNAs based on a threshold of $p < 0.05$. The target gene candidates of differentially expressed miRNAs were subjected to Gene Ontology (GO) enrichment analysis using the GO database (http://www.geneontology.org/). Furthermore, the Kyoto Encyclopedia of Genes and Genomes (KEGG) ortholog-based annotation system software was used to assess the statistical enrichment of target genes in KEGG pathways.[86]

Human serum and pancreatic sample collection

Human serum samples were collected from a cohort of 43 patients diagnosed with CP (mean age, 43.75 ± 11.77 years) who participated in Medical University of South Carolina (MUSC)-Institutional Review Board (IRB)-approved clinical trials (IRB protocol # Pro00053906). Written consent was obtained from each participant before the study. Additionally, human CP and healthy pancreas tissues were obtained from the MUSC biorepository without identifiable information. The IRB determined this portion to be a non-human subject study.

CP induction in mice

We purchased male C57BL/6 mice (10–12 weeks old) from the Jackson Laboratory. CP was induced in the mice by administering a single infusion of 0.4% TNBS (50 μL) dissolved in ethanol (10%, v/v) via the bile duct, following established protocols.[13] Ethical approval for all experimental procedures was obtained from the Institutional Animal Care and Use Committee of the MUSC. Non-invasive and

painless methods that use tail staining with dyes or markers were used for identifying individual mice in each group to minimize the effect of their condition and the physiological outcomes of disease modeling.[87]

Pain assessment

Mechanical sensitivity in the paw and abdominal areas was measured by applying calibrated von Frey filament (North Coast Medical) with gradually increasing forces.[28,88] The application was repeated 10 times for 1–2 s each. A positive response was documented when the mouse exhibited behaviors such as raising, retracting, or licking the abdominal area. The data represent the average minimum applied force by the calibrated vFF that triggered a positive response for each mouse within the experimental groups. All evaluations were carried out blindly.

Behavior test by the open field assessment

Hyperactivity and anxious behaviors were assessed using the open field test.[89] The open field apparatus comprised a plexiglass square box measuring 60 cm × 60 cm × 25 cm, with a designated center area marked. Each animal was individually placed in the box for 10 min. The movements and behaviors of all animals were recorded using a digital camera and subsequently analyzed using Noldus's Ethovision system. The parameters studied included the time spent and distance traveled within the center area and the average velocity.

Histopathological scoring of the pancreas

Pancreas tissues were fixed in paraffin, sectioned into 5-μm slices, and stained with H&E and Masson's trichrome. The sections were then examined by a pathologist blinded to the experimental groups. The pathologist assessed the severity of pancreatitis in four categories: inflammation, necrosis, fibrosis, acinar cells, and interlobular edema, using a scoring system ranging from 0 to 5.[90] The total preserved area was evaluated based on the histological features observed throughout the slide, expressed as a percentage from 0% to 100%. The Keyence microscope BZ-X800 was utilized for slide scanning during this process.

Immunohistochemistry

Pancreases from treated mice were preserved in paraffin, while DRG samples were embedded in an optimal cutting temperature compound (OCT; Sakura Finetek); both were sectioned into 5-μm slices. Immunostaining was performed using primary antibodies specific to ferroptosis pathways, fibrosis (α-SMA), pain/macrophage (TRPV1, c-FOS, and CD68) markers, and secondary antibodies listed in Table S1. The slides were visualized using an Invitrogen EVOS M5000 Fluorescence Microscope (Thermo Fisher Scientific), photos were taken under the same exposure conditions, and staining integrated density was quantified using ImageJ software (NIH).

Detection of mast cells

Paraffin-embedded pancreatic samples and OCT-embedded DRG tissues underwent May-Grünwald-Giemsa staining following the manufacturer's recommendations (Eng Scientific). The staining process involved deparaffinization, treatment with May-Grünwald Solution and Giemsa stain, washing with PBS, dehydration with ethanol, and clearing with xylene. Mast cells were then quantified in 10 randomized fields per section using a light microscope, and the results were reported as mast cells per square millimeter.

Iron deposition in the pancreas

Prussian blue staining was utilized to evaluate the presence of intracellular iron in pancreatic samples.[53] The process involved deparaffinizing the sections, followed by staining with an iron stain solution according to the manufacturer's instructions (Iron Stain Kit; Abcam). Subsequently, nuclear staining with a fast red solution, dehydration in ethanol, and resin mounting were carried out. The identification of blue intracellular particles indicates the presence of iron, and the density of iron-positive cells was determined by examining five randomly selected fields of view per sample under a light microscope.

GSH and GPx activity assay

The concentrations of GSH in mouse serum and the activity of GPx in mouse pancreas tissue lysates and human serum samples were determined using separate colorimetric assay kits (Abcam), following the provided protocols. Briefly, the serum samples were deproteinized and incubated with the GSH Assay mixture for 60 min at room temperature. The GSH concentration was determined as the absorbance value of each sample at 490/520 nm using a microplate reader (Bio-Rad Laboratories). For GPx activity, the samples were incubated with GSH reductase and GSH for 15 min to deplete all GSSG and then incubated with cumene hydroperoxide. The absorbance measured at 340 nm was a direct proportion of GPx activity.

Serum amylase assay

Human blood samples were centrifuged at 4°C for 15 min at 1,300×*g* to separate the serum. Amylase concentrations were measured using an Amylase Activity Assay kit obtained from Sigma-Aldrich, following the manufacturer's instructions.

Iron assay

Serum iron concentration was measured using the Iron Assay kit (Abcam) following the manufacturer's protocol. Briefly, serum samples were incubated with the working solution at 37°C for 30 min, followed by 60 min at the same temperature with the iron probe. The resulting output was measured immediately using a colorimetric microplate reader, with the absorbance read at 593 nm.

Lipid peroxidation assay

The concentration of MDA in pancreas lysates was assessed using the Lipid Peroxidation Assay Kit (Abcam) according to the manufacturer's instructions. Briefly, samples were subjected to a reaction with thiobarbituric acid at 95°C for 60 min. The resulting product was then quantified by measuring the absorbance at 352 nm using a microplate reader.

Real-time qPCR

Total RNA was extracted from the pancreas and DRG tissues using an RNA extraction kit (Qiagen). Subsequently, the RNA was utilized to synthesize cDNA with the iScript cDNA Synthesis Kit (Bio-Rad) on an Applied Biosystems Veriti 96-Well Thermal Cycler (Thermo Fisher Scientific). Real-time PCR was conducted in triplicate using specific primer pairs (Table S2), the CFX-96 real-time PCR system thermal cycler, and SYBR Green Mastermix (Bio-Rad). The expression levels of β-actin or GAPDH were employed to normalize the gene expression levels. The qPCR data were subsequently analyzed using the LightCycler 96 Relative Quantification software (Bio-Rad).

Western blot

Total proteins from the mouse pancreas were lysed in a protein lysis buffer containing a protease and phosphatase inhibitor cocktail (Sigma-Aldrich). Protein concentrations were determined using the BCA protein assay kit (Thermo Fisher Scientific). An equivalent amount (20 μg) of protein was loaded and separated by electrophoresis on a 10% SDS-PAGE gel and transferred onto nitrocellulose membranes. The membranes were blocked and incubated with primary antibodies (Table S1) overnight at 4°C. The next day, the membranes were washed thrice and incubated with the corresponding secondary antibodies at room temperature for 1 h. Finally, the blots were imaged using a ChemiDocTM Imaging System (Bio-Rad) and analyzed using ImageJ software. β-actin was used as a loading control.

Statistical analysis

Data were presented as means ± SD and analyzed using the GraphPad Prism software (Version 9). Statistical comparisons among groups were performed using one-way ANOVA followed by a post-hoc analysis. A p value of ≤ 0.05 was considered statistically significant.

DATA AVAILABILITY

The data supporting this study's findings are available from the corresponding author upon reasonable request.

ACKNOWLEDGMENTS

The National Institutes of Health supported this study (R01DK105183, R01DK120394, and R01DK125464). We thank Mr. Michael Lee for critical language editing. Some illustrations were prepared using Biorender software.

AUTHOR CONTRIBUTIONS

S.S. and H.W. designed the experiments. S.S., W.G., T.Y., K.H., and E.G. performed the experiments. S.S. analyzed the data. S.S., C.S., and H.W. wrote the manuscript.

DECLARATION OF INTERESTS

The authors declare no competing interests.

SUPPLEMENTAL INFORMATION

Supplemental information can be found online at https://doi.org/10.1016/j.ymthe.2025.03.028.

REFERENCES

1. Yadav, D., and Lowenfels, A.B. (2013). The epidemiology of pancreatitis and pancreatic cancer. Gastroenterology *144*, 1252–1261. https://doi.org/10.1053/j.gastro.2013.01.068.

2. Sun, Z., Gou, W., Kim, D.S., Dong, X., Strange, C., Tan, Y., Adams, D.B., and Wang, H. (2017). Adipose Stem Cell Therapy Mitigates Chronic Pancreatitis via Differentiation into Acinar-like Cells in Mice. Mol. Ther. *25*, 2490–2501. https://doi.org/10.1016/j.ymthe.2017.06.016.

3. Kong, L., Xu, X., Zhang, H., Zhou, Y., Huang, H., Chen, B., and Zhou, Z. (2021). Human umbilical cord-derived mesenchymal stem cells improve chronic pancreatitis in rats via the AKT-mTOR-S6K1 signaling pathway. Bioengineered *12*, 1986–1996. https://doi.org/10.1080/21655979.2021.1928441.

4. Brock, C., Nielsen, L.M., Lelic, D., and Drewes, A.M. (2013). Pathophysiology of chronic pancreatitis. World J. Gastroenterol. *19*, 7231–7240. https://doi.org/10.3748/wjg.v19.i42.7231.

5. Jiang, X., Stockwell, B.R., and Conrad, M. (2021). Ferroptosis: mechanisms, biology and role in disease. Nat. Rev. Mol. Cell Biol. *22*, 266–282. https://doi.org/10.1038/s41580-020-00324-8.

6. Hu, W., Liang, K., Zhu, H., Zhao, C., Hu, H., and Yin, S. (2022). Ferroptosis and Its Role in Chronic Diseases. Cells *11*, 2040. https://doi.org/10.3390/cells11132040.

7. Mancias, J.D., and Kimmelman, A.C. (2016). Mechanisms of Selective Autophagy in Normal Physiology and Cancer. J. Mol. Biol. *428*, 1659–1680. https://doi.org/10.1016/j.jmb.2016.02.027.

8. Wang, X., Liu, Z., Peng, P., Gong, Z., Huang, J., and Peng, H. (2022). Astaxanthin attenuates osteoarthritis progression via inhibiting ferroptosis and regulating mitochondrial function in chondrocytes. Chem. Biol. Interact. *366*, 110148. https://doi.org/10.1016/j.cbi.2022.110148.

9. Liu, K., Liu, J., Zou, B., Li, C., Zeh, H.J., Kang, R., Kroemer, G., Huang, J., and Tang, D. (2022). Trypsin-Mediated Sensitization to Ferroptosis Increases the Severity of Pancreatitis in Mice. Cell. Mol. Gastroenterol. Hepatol. *13*, 483–500. https://doi.org/10.1016/j.jcmgh.2021.09.008.

10. Fan, R., Sui, J., Dong, X., Jing, B., and Gao, Z. (2021). Wedelolactone alleviates acute pancreatitis and associated lung injury via GPX4 mediated suppression of pyroptosis and ferroptosis. Free Radic. Biol. Med. *173*, 29–40. https://doi.org/10.1016/j.freeradbiomed.2021.07.009.

11. Li, S., Zhang, G., Wang, M., Shen, H., Li, X., Li, X., Li, W., Xiao, Y., Wang, S., and Liu, H. (2022). Chaihu Guizhi Decoction (CGD) ameliorates chronic pancreatitis (CP) -induced mechanical allodynia by inhibiting microglia P2X7R-NLRP3 inflammasome activation. Preprint at J. Evid. Based Complementary Altern. Med. https://doi.org/10.21203/rs.3.rs-2250306/v1.

12. Jaster, R., and Emmrich, J. (2008). Crucial role of fibrogenesis in pancreatic diseases. Best Pract. Res. Clin. Gastroenterol. *22*, 17–29. https://doi.org/10.1016/j.bpg.2007.10.004.

13. Gou, W., Swaby, L., Marissa Wolfe, A., Lancaster, W.P., Morgan, K.A., and Wang, H. (2022). A Mouse Model for Chronic Pancreatitis via Bile Duct TNBS Infusion. J. Vis. Exp. e62080. https://doi.org/10.3791/62080.

14. Poulsen, J.L., Schou Olesen, S., Malver, L.P., Frøkjær, J.B., and Drewes, A.M. (2013). Pain and chronic pancreatitis: A complex interplay of multiple mechanisms. World J. Gastroenterol. *19*, 7282–7291. https://doi.org/10.3748/wjg.v19.

15. Glaubitz, J., Wilden, A., Golchert, J., Homuth, G., Völker, U., Bröker, B.M., Thiele, T., Lerch, M.M., Mayerle, J., Aghdassi, A.A., et al. (2022). In mouse chronic pancreatitis CD25(+)FOXP3(+) regulatory T cells control pancreatic fibrosis by suppression of the type 2 immune response. Nat. Commun. *13*, 4502. https://doi.org/10.1038/s41467-022-32195-2.

16. Thery, C., Zitvogel, L., and Amigorena, S. (2002). Exosomes: composition, biogenesis and function. Nat. Rev. Immunol. *2*, 569–579. https://doi.org/10.1038/nri855.

17. Nikfarjam, S., Rezaie, J., Zolbanin, N.M., and Jafari, R. (2020). Mesenchymal stem cell derived-exosomes: a modern approach in translational medicine. J. Transl. Med. *18*, 449. https://doi.org/10.1186/s12967-020-02622-3.

18. Yu, M., Liu, W., Li, J., Lu, J., Lu, H., Jia, W., and Liu, F. (2020). Exosomes derived from atorvastatin-pretreated MSC accelerate diabetic wound repair by enhancing

angiogenesis via AKT/eNOS pathway. Stem Cell Res. Ther. *11*, 350. https://doi.org/10.1186/s13287-020-01824-2.

19. Zargar, M.J., Kaviani, S., Vasei, M., Soufi Zomorrod, M., Heidari Keshel, S., and Soleimani, M. (2022). Therapeutic role of mesenchymal stem cell-derived exosomes in respiratory disease. Stem Cell Res. Ther. *13*, 194. https://doi.org/10.1186/s13287-022-02866-4.

20. Zheng, Y., Sun, W., Shan, C., Li, B., Liu, J., Xing, H., Xu, Q., Cui, B., Zhu, W., Chen, J., et al. (2022). beta-hydroxybutyrate inhibits ferroptosis-mediated pancreatic damage in acute liver failure through the increase of H3K9bhb. Cell Rep. *41*, 111847. https://doi.org/10.1016/j.celrep.2022.111847.

21. Gatti, S., Bruno, S., Deregibus, M.C., Sordi, A., Cantaluppi, V., Tetta, C., and Camussi, G. (2011). Microvesicles derived from human adult mesenchymal stem cells protect against ischaemia-reperfusion-induced acute and chronic kidney injury. Nephrol. Dial. Transpl. *26*, 1474–1483. https://doi.org/10.1093/ndt/gfr015.

22. Papadakos, S.P., Dedes, N., Pergaris, A., Gazouli, M., and Theocharis, S. (2022). Exosomes in the Treatment of Pancreatic Cancer: A Moonshot to PDAC Treatment? Int. J. Mol. Sci. *23*, 3620. https://doi.org/10.3390/ijms23073620.

23. Jing, S., Lu, Y., Zhang, J., Ren, Y., Mo, Y., Liu, D., Duan, L., Yuan, Z., Wang, C., and Wang, Q. (2022). Levistilide a Induces Ferroptosis by Activating the Nrf2/HO-1 Signaling Pathway in Breast Cancer Cells. Drug Des. Devel. Ther. *16*, 2981–2993. https://doi.org/10.2147/DDDT.S374328.

24. Song, L., Gou, W., Wang, J., Wei, H., Lee, J., Strange, C., and Wang, H. (2021). Overexpression of alpha-1 antitrypsin in mesenchymal stromal cells improves their intrinsic biological properties and therapeutic effects in nonobese diabetic mice. Stem Cells Transl. Med. *10*, 320–331. https://doi.org/10.1002/sctm.20-0122.

25. Koulmanda, M., Bhasin, M., Hoffman, L., Fan, Z., Qipo, A., Shi, H., Bonner-Weir, S., Putheti, P., Degauque, N., Libermann, T.A., et al. (2008). Curative and beta cell regenerative effects of alpha1-antitrypsin treatment in autoimmune diabetic NOD mice. Proc. Natl. Acad. Sci. *105*, 16242–16247.

26. Liu, T.M., Ng, W.M., Tan, H.S., Vinitha, D., Yang, Z., Fan, J.B., Zou, Y., Hui, J.H., Lee, E.H., and Lim, B. (2013). Molecular basis of immortalization of human mesenchymal stem cells by combination of p53 knockdown and human telomerase reverse transcriptase overexpression. Stem Cells Dev. *22*, 268–278. https://doi.org/10.1089/scd.2012.0222.

27. Cattaruzza, F., Johnson, C., Leggit, A., Grady, E., Schenk, A.K., Cevikbas, F., Cedron, W., Bondada, S., Kirkwood, R., Malone, B., et al. (2013). Transient receptor potential ankyrin 1 mediates chronic pancreatitis pain in mice. Am. J. Physiol. Gastrointest. Liver Physiol. *304*, G1002–G1012. https://doi.org/10.1152/ajpgi.00005.2013.

28. Chow, R.P., Nguyen, K., Gou, W., Green, E., Morgan, K., Lancaster, W., Helke, K., Strange, C., and Wang, H. (2021). A Novel Cellular Therapy to Treat Pancreatic Pain in Experimental Chronic Pancreatitis Using Human Alpha-1 Antitrypsin Overexpressing Mesenchymal Stromal Cells. Biomedicines *9*, 1695. https://doi.org/10.3390/biomedicines9111695.

29. El-Benhawy, S.A., Abdelrhman, I.G., Sadek, N.A., Fahmy, E.I., AboGabal, A.A., Elmasry, H., Saleh, S.A.M., Sakr, O.A., Elwany, M.N., and Rabie, M.A.F. (2023). Studying ferroptosis and iron metabolism pre- and post-radiotherapy treatment in breast cancer patients. J. Egypt. Natl. Canc. Inst. *35*, 4. https://doi.org/10.1186/s43046-023-00162-7.

30. Cui, C., Zang, N., Song, J., Guo, X., He, Q., Hu, H., Yang, M., Wang, Y., Yang, J., Zou, Y., et al. (2022). Exosomes derived from mesenchymal stem cells attenuate diabetic kidney disease by inhibiting cell apoptosis and epithelial-to-mesenchymal transition via miR-424-5p. FASEB J. *36*, e22517. https://doi.org/10.1096/fj.202200488R.

31. Santana-Codina, N., and Mancias, J.D. (2018). The Role of NCOA4-Mediated Ferritinophagy in Health and Disease. Pharmaceuticals (Basel) *11*, 114. https://doi.org/10.3390/ph11040114.

32. Chen, Z., Jiang, J., Fu, N., and Chen, L. (2022). Targetting ferroptosis for blood cell-related diseases. J. Drug Target. *30*, 244–258. https://doi.org/10.1080/1061186X.2021.1971237.

33. Yan, H.F., Zou, T., Tuo, Q.Z., Xu, S., Li, H., Belaidi, A.A., and Lei, P. (2021). Ferroptosis: mechanisms and links with diseases. Signal Transduct. Target. Ther. *6*, 49. https://doi.org/10.1038/s41392-020-00428-9.

34. Li, H., Lin, Y., Zhang, L., Zhao, J., and Li, P. (2022). Ferroptosis and its emerging roles in acute pancreatitis. Chin. Med. J. *135*, 2026–2034. https://doi.org/10.1097/CM9.0000000000002096.

35. Chen, S., Zhu, J.Y., Zang, X., and Zhai, Y.Z. (2021). The Emerging Role of Ferroptosis in Liver Diseases. Front. Cell Dev. Biol. *9*, 801365. https://doi.org/10.3389/fcell.2021.801365.

36. Dworzanski, J., Strycharz-Dudziak, M., Kliszczewska, E., Kielczykowska, M., Dworzanska, A., Drop, B., and Polz-Dacewicz, M. (2020). Glutathione peroxidase (GPx) and superoxide dismutase (SOD) activity in patients with diabetes mellitus type 2 infected with Epstein-Barr virus. PLoS One *15*, e0230374. https://doi.org/10.1371/journal.pone.0230374.

37. Chen, J., Wang, Y., Wu, J., Yang, J., Li, M., and Chen, Q. (2020). The Potential Value of Targeting Ferroptosis in Early Brain Injury After Acute CNS Disease. Front. Mol. Neurosci. *13*, 110. https://doi.org/10.3389/fnmol.2020.00110.

38. Xu, C., Shen, J., Zhang, J., Jia, Z., He, Z., Zhuang, X., Xu, T., Shi, Y., Zhu, S., Wu, M., and Han, W. (2015). Recombinant interleukin-1 receptor antagonist attenuates the severity of chronic pancreatitis induced by TNBS in rats. Biochem. Pharmacol. *93*, 449–460. https://doi.org/10.1016/j.bcp.2014.12.016.

39. Yang, L., Shen, J., He, S., Hu, G., Shen, J., Wang, F., Xu, L., Dai, W., Xiong, J., Ni, J., et al. (2012). L-cysteine administration attenuates pancreatic fibrosis induced by TNBS in rats by inhibiting the activation of pancreatic stellate cell. PLoS One *7*, e31807. https://doi.org/10.1371/journal.pone.0031807.

40. O'Sullivan, S., Gilmer, J.F., and Medina, C. (2015). Matrix metalloproteinases in inflammatory bowel disease: an update. Mediators Inflamm. *2015*, 964131. https://doi.org/10.1155/2015/964131.

41. Christakis, D.A., Ramirez, J.S.B., and Ramirez, J.M. (2012). Overstimulation of newborn mice leads to behavioral differences and deficits in cognitive performance. Sci. Rep. *2*, 546. https://doi.org/10.1038/srep00546.

42. Hashimoto, A., Karim, M.R., Kuramochi, M., Izawa, T., Kuwamura, M., and Yamate, J. (2020). Characterization of Macrophages and Myofibroblasts Appearing in Dibutyltin Dichloride-Induced Rat Pancreatic Fibrosis. Toxicol. Pathol. *48*, 509–523. https://doi.org/10.1177/0192623319893310.

43. Beaudry, K.L., Parsons, C.L.M., Ellis, S.E., and Akers, R.M. (2016). Localization and quantitation of macrophages, mast cells, and eosinophils in the developing bovine mammary gland. J. Dairy Sci. *99*, 796–804. https://doi.org/10.3168/jds.2015-9972.

44. Hoogerwerf, W.A., Gondesen, K., Xiao, S.Y., Winston, J.H., Willis, W.D., and Pasricha, P.J. (2005). The role of mast cells in the pathogenesis of pain in chronic pancreatitis. BMC Gastroenterol. *5*, 8. https://doi.org/10.1186/1471-230X-5-8.

45. Staton, P.C., Wilson, A.W., Bountra, C., Chessell, I.P., and Day, N.C. (2007). Changes in dorsal root ganglion CGRP expression in a chronic inflammatory model of the rat knee joint: differential modulation by rofecoxib and paracetamol. Eur. J. Pain *11*, 283–289. https://doi.org/10.1016/j.ejpain.2006.03.006.

46. Romero, A., González-Cuello, A., Laorden, M.L., Campillo, A., Vasconcelos, N., Romero-Alejo, E., and Puig, M.M. (2012). Effects of surgery and/or remifentanil administration on the expression of pERK1/2, c-Fos and dynorphin in the dorsal root ganglia in mice. Naunyn. Schmiedebergs. Arch. Pharmacol. *385*, 397–409. https://doi.org/10.1007/s00210-011-0721-z.

47. Barik, A., Sathyamurthy, A., Thompson, J., Seltzer, M., Levine, A., and Chesler, A. (2021). A spinoparabrachial circuit defined by Tacr1 expression drives pain. Elife *10*, e61135. https://doi.org/10.7554/eLife.61135.

48. Zhang, M.D., Tortoriello, G., Hsueh, B., Tomer, R., Ye, L., Mitsios, N., Borgius, L., Grant, G., Kiehn, O., Watanabe, M., et al. (2014). Neuronal calcium-binding proteins 1/2 localize to dorsal root ganglia and excitatory spinal neurons and are regulated by nerve injury. Proc. Natl. Acad. Sci. USA *111*, E1149–E1158. https://doi.org/10.1073/pnas.1402318111.

49. Shen, Z., Huang, W., Liu, J., Tian, J., Wang, S., and Rui, K. (2021). Effects of Mesenchymal Stem Cell-Derived Exosomes on Autoimmune Diseases. Front. Immunol. *12*, 749192. https://doi.org/10.3389/fimmu.2021.749192.

50. Tamura, R., Uemoto, S., and Tabata, Y. (2016). Immunosuppressive effect of mesenchymal stem cell-derived exosomes on a concanavalin A-induced liver injury model. Inflamm. Regen. *36*, 26. https://doi.org/10.1186/s41232-016-0030-5.

51. Liu, H., Liang, Z., Wang, F., Zhou, C., Zheng, X., Hu, T., He, X., Wu, X., and Lan, P. (2019). Exosomes from mesenchymal stromal cells reduce murine colonic

inflammation via a macrophage-dependent mechanism. JCI Insight *4*, e131273. https://doi.org/10.1172/jci.insight.131273.

52. Xu, J., Liu, S., Cui, Z., Wang, X., Ning, T., Wang, T., Zhang, N., Xie, S., Min, L., Zhang, S., et al. (2021). Ferrostatin-1 alleviated TNBS induced colitis via the inhibition of ferroptosis. Biochem. Biophys. Res. Commun. *573*, 48–54. https://doi.org/10.1016/j.bbrc.2021.08.018.

53. Stancic, A., Saksida, T., Markelic, M., Vucetic, M., Grigorov, I., Martinovic, V., Gajic, D., Ivanovic, A., Velickovic, K., Savic, N., and Otasevic, V. (2022). Ferroptosis as a Novel Determinant of beta-Cell Death in Diabetic Conditions. Oxid. Med. Cell. Longev. *2022*, 3873420. https://doi.org/10.1155/2022/3873420.

54. Dai, E., Han, L., Liu, J., Xie, Y., Zeh, H.J., Kang, R., Bai, L., and Tang, D. (2020). Ferroptotic damage promotes pancreatic tumorigenesis through a TMEM173/STING-dependent DNA sensor pathway. Nat. Commun. *11*, 6339. https://doi.org/10.1038/s41467-020-20154-8.

55. Xu, X.F., Fan, J.W., Xin, J.Q., Wu, N., Gao, H., Duan, L.F., Zou, W.B., Zhang, H., and Li, Z.S. (2022). Aspirin Ameliorates Pancreatic Inflammation and Fibrosis by Inhibiting COX-2 Expression in Experimental Chronic Pancreatitis. J. Inflamm. Res. *15*, 4737–4749. https://doi.org/10.2147/JIR.S375383.

56. Chen, J., Crawford, R., Chen, C., and Xiao, Y. (2013). The key regulatory roles of the PI3K/Akt signaling pathway in the functionalities of mesenchymal stem cells and applications in tissue regeneration. Tissue Eng. Part B Rev. *19*, 516–528. https://doi.org/10.1089/ten.TEB.2012.0672.

57. Gao, S., Chen, B., Zhu, Z., Du, C., Zou, J., Yang, Y., Huang, W., and Liao, J. (2023). PI3K-Akt signaling regulates BMP2-induced osteogenic differentiation of mesenchymal stem cells (MSCs): A transcriptomic landscape analysis. Stem Cell Res. *66*, 103010. https://doi.org/10.1016/j.scr.2022.103010.

58. Hendrickx, D.A.E., van Eden, C.G., Schuurman, K.G., Hamann, J., and Huitinga, I. (2017). Staining of HLA-DR, Iba1 and CD68 in human microglia reveals partially overlapping expression depending on cellular morphology and pathology. J. Neuroimmunol. *309*, 12–22. https://doi.org/10.1016/j.jneuroim.2017.04.007.

59. Zhang, K., Wu, L., Zhang, P., Luo, M., Du, J., Gao, T., O'Connell, D., Wang, G., Wang, H., and Yang, Y. (2018). miR-9 regulates ferroptosis by targeting glutamic-oxaloacetic transaminase GOT1 in melanoma. Mol. Carcinog. *57*, 1566–1576. https://doi.org/10.1002/mc.22878.

60. Bin, S., Xin, L., Lin, Z., Jinhua, Z., Rui, G., and Xiang, Z. (2021). Targeting miR-10a-5p/IL-6R axis for reducing IL-6-induced cartilage cell ferroptosis. Exp. Mol. Pathol. *118*, 104570. https://doi.org/10.1016/j.yexmp.2020.104570.

61. Luo, Y., Chen, Y., Jin, H., Hou, B., Li, H., Li, X., Liu, L., Zhou, Y., Li, Y., Song, Y.S., et al. (2023). The suppression of cervical cancer ferroptosis by macrophages: The attenuation of ALOX15 in cancer cells by macrophages-derived exosomes. Acta Pharm. Sin. B *13*, 2645–2662. https://doi.org/10.1016/j.apsb.2023.03.025.

62. Yang, R., Zhou, S., Huang, J., Kang, D., Chen, Y., Wang, X., Shi, Y., and Wang, Z. (2024). The role of Q10 engineering mesenchymal stem cell-derived exosomes in inhibiting ferroptosis for diabetic wound healing. Burns Trauma *12*, tkae054. https://doi.org/10.1093/burnst/tkae054.

63. Li, Y., Liu, J., Zhang, J., Zhang, W., and Wu, Z. (2020). Characterization of microRNA profile in IgE-mediated mouse BMMCs degranulation. J. Microbiol. Immunol. Infect. *53*, 550–560. https://doi.org/10.1016/j.jmii.2018.10.006.

64. Hu, F., Lou, N., Jiao, J., Guo, F., Xiang, H., and Shang, D. (2020). Macrophages in pancreatitis: Mechanisms and therapeutic potential. Biomed. Pharmacother. *131*, 110693. https://doi.org/10.1016/j.biopha.2020.110693.

65. Yu, D., Zhu, J., Zhu, M., Wei, K., Chen, Q., Wu, X., Miao, X., and Lu, Z. (2019). Inhibition of Mast Cell Degranulation Relieves Visceral Hypersensitivity Induced by Pancreatic Carcinoma in Mice. J. Mol. Neurosci. *69*, 235–245. https://doi.org/10.1007/s12031-019-01352-6.

66. Rusca, N., Dehò, L., Montagner, S., Zielinski, C.E., Sica, A., Sallusto, F., and Monticelli, S. (2012). MiR-146a and NF-κB1 regulate mast cell survival and T lymphocyte differentiation. Mol. Cell. Biol. *32*, 4432–4444. https://doi.org/10.1128/mcb.00824-12.

67. Poya, M.N., Hausser, J., Trajkovski, M., Braun, M., Collins, S., Rorsman, P., Zavolan, M., and Stoffel, M. (2009). miR-375 maintains normal pancreatic α- and β-cell mass. PNAS *106*, 5813–5818.

68. Zhan, Y., Chen, C., Wu, Z., Zhou, F., and Yu, X. (2023). miR-455-3p ameliorates pancreatic acinar cell injury by targeting Slc2a1. PeerJ *11*, e15612. https://doi.org/10.7717/peerj.15612.

69. Dey, S., Udari, L.M., RiveraHernandez, P., Kwon, J.J., Willis, B., Easler, J.J., Fogel, E. L., Pandol, S., and Kota, J. (2021). Loss of miR-29a/b1 promotes inflammation and fibrosis in acute pancreatitis. JCI Insight *6*, e149539. https://doi.org/10.1172/jci.insight.149539.

70. Ma, Y., Shen, N., Wicha, M.S., and Luo, M. (2021). The Roles of the Let-7 Family of MicroRNAs in the Regulation of Cancer Stemness. Cells *10*, 2415. https://doi.org/10.3390/cells10092415.

71. Zhang, S., Liu, X., Wang, J., Yuan, F., and Liu, Y. (2022). Targeting ferroptosis with miR-144-3p to attenuate pancreatic beta cells dysfunction via regulating USP22/SIRT1 in type 2 diabetes. Diabetol. Metab. Syndr. *14*, 89. https://doi.org/10.1186/s13098-022-00852-7.

72. Aguiar Koga, B.A., Fernandes, L.A., Fratini, P., Sogayar, M.C., and Carreira, A.C.O. (2022). Role of MSC-derived small extracellular vesicles in tissue repair and regeneration. Front. Cell Dev. Biol. *10*, 1047094. https://doi.org/10.3389/fcell.2022.1047094.

73. Kou, M., Huang, L., Yang, J., Chiang, Z., Chen, S., Liu, J., Guo, L., Zhang, X., Zhou, X., Xu, X., et al. (2022). Mesenchymal stem cell-derived extracellular vesicles for immunomodulation and regeneration: a next generation therapeutic tool? Cell Death Dis. *13*, 580. https://doi.org/10.1038/s41419-022-05034-x.

74. Manzoor, T., Saleem, A., Farooq, N., Dar, L.A., Nazir, J., Saleem, S., Ismail, S., Gugjoo, M.B., Shiekh, P.A., and Ahmad, S.M. (2023). Extracellular vesicles derived from mesenchymal stem cells — a novel therapeutic tool in infectious diseases. Inflamm. Regen. *43*, 17. https://doi.org/10.1186/s41232-023-00266-6.

75. Welsh, J.A., Goberdhan, D.C.I., O'Driscoll, L., Buzas, E.I., Blenkiron, C., Bussolati, B., Cai, H., Di Vizio, D., Driedonks, T.A.P., Erdbrügger, U., et al. (2024). Minimal information for studies of extracellular vesicles (MISEV2023): From basic to advanced approaches. J. Extracell. Vesicles *13*, e12404. https://doi.org/10.1002/jev2.12404.

76. Lotfy, A., AboQuella, N.M., and Wang, H. (2023). Mesenchymal stromal/stem cell (MSC)-derived exosomes in clinical trials. Stem Cell Res. Ther. *14*, 66. https://doi.org/10.1186/s13287-023-03287-7.

77. Shoeibi, S., Green, E., Wei, H., Gou, W., Strange, C., and Wang, H. (2024). Immortalized mesenchymal stromal cells overexpressing alpha-1 antitrypsin protect acinar cells from apoptotic and ferroptotic cell death. J. Cell. Mol. Med. *28*, e70093. https://doi.org/10.1111/jcmm.70093.

78. Tong, Y., Sun, J., Jiang, X., Jia, X., Xiao, H., Wang, H., and Yang, G. (2025). A study on the production of extracellular vesicles derived from novel immortalized human placental mesenchymal stromal cells. Sci. Rep. *15*, 3568. https://doi.org/10.1038/s41598-025-87371-3.

79. Brancolini, A., Bobbili, M.R., Pultar, M., Mazidi, Z., Wieser, M., Gamauf, J., Roefs, M.T., Corso, G., Nivarthi, H., Paredes, M.B.A., et al. (2024). Immortalization of mesenchymal stromal cells by hTERT does not affect the functional properties of secreted extracellular vesicles. Preprint at bioRxiv. https://doi.org/10.1101/2024.12.05.626964.

80. Chen, Z., Meng, D., Pang, X., Guo, J., Li, T., Song, J., and Peng, Y. (2024). Deer antler stem cells immortalization by modulation of hTERT and the small extracellular vesicles characters. Front. Vet. Sci. *11*, 1440855. https://doi.org/10.3389/fvets.2024.1440855.

81. Langmead, B., Trapnell, C., Pop, M., and Salzberg, S.L. (2009). Ultrafast and memory-efficient alignment of short DNA sequences to the human genome. Genome Biol. *10*, R25.

82. Friedländer, M.R., Mackowiak, S.D., Li, N., Chen, W., and Rajewsky, N. (2012). miRDeep2 accurately identifies known and hundreds of novel microRNA genes in seven animal clades. Nucleic Acids Res. *40*, 37–52.

83. Wen, M., Shen, Y., Shi, S., and Tang, T. (2012). miREvo: an integrative microRNA evolutionary analysis platform for next-generation sequencing experiments. BMC Bioinformatics *13*, 140.

84. Enright, A.J., John, B., Gaul, U., Tuschl, T., Sander, C., and Marks, D.S. (2003). MicroRNA targets in Drosophila. Genome Biol. *5*, R1.

85. Zhou, L., Chen, J., Li, Z., Li, X., Hu, X., Huang, Y., Zhao, X., Liang, C., Wang, Y., Sun, L., et al. (2010). Integrated profiling of microRNAs and mRNAs: microRNAs located on Xq27.3 associate with clear cell renal cell carcinoma. PLoS One *5*, e15224. https://doi.org/10.1371/journal.pone.0015224.

86. Mao, X., Cai, T., Olyarchuk, J.G., and Wei, L. (2005). Automated genome annotation and pathway identification using the KEGG Orthology (KO) as a controlled vocabulary. Bioinformatics *21*, 3787–3793.

87. Klabukov, I., Shestakova, V., Krasilnikova, O., Smirnova, A., Abramova, O., Baranovskii, D., Atiakshin, D., Kostin, A.A., Shegay, P., and Kaprin, A.D. (2023). Refinement of Animal Experiments: Replacing Traumatic Methods of Laboratory Animal Marking with Non-Invasive Alternatives. Animals *13*, 3452. https://doi.org/10.3390/ani13223452.

88. Winston, J.H., He, Z.J., Shenoy, M., Xiao, S.Y., and Pasricha, P.J. (2005). Molecular and behavioral changes in nociception in a novel rat model of chronic pancreatitis for the study of pain. Pain *117*, 214–222. https://doi.org/10.1016/j.pain.2005.06.013.

89. de Lombares, C., Heude, E., Alfama, G., Fontaine, A., Hassouna, R., Vernochet, C., de Chaumont, F., Olivo-Marin, C., Ey, E., Parnaudeau, S., et al. (2019). Dlx5 and Dlx6 expression in GABAergic neurons controls behavior, metabolism, healthy aging and lifespan. Aging (Albany NY) *11*, 6638–6656. https://doi.org/10.18632/aging.102141.

90. Fukumura, Y. (2007). Histological Characteristics of Chronic Pancreatitis, Based upon Etiology. In Pancreas Pathological Practice and Research, K. Suda, ed. (Karger), pp. 146–153.